Supporting information

for

Coordination of Ru-arene fragments to dipyridophenazine ligands leads to the modulation of their *in vitro* and *in vivo* anticancer activity

Stefan Nikolić,[†] Jemma Arakelyan,[‡] Vladimir Kushnarev,[‡] Samah Mutasim Alfadul,[‡] Dalibor Stanković,[§] Yaroslav I. Kraynik,[‡] Sanja Grgurić-Šipka[§,*] Maria V. Babak [‡,*]

[†] Innovative Centre of thr Faculty of Chemistry Belgrade, University of Belgrade, Studentski trg 12‑16,11000 Belgrade, Serbia

[‡]Drug Discovery Lab, Department of Chemistry, City University of Hong Kong, 83 Tat Chee Avenue, Hong Kong SAR, 999077, People's Republic of China

[§]University of Belgrade, Faculty of Chemistry, Studentski trg 12-16, 11000 Belgrade, Serbia

* corresponding authors

E-mail address: sanjag@chem.bg.ac.rs (SGS), mbabak@cityu.edu.hk (MVB)

Table of contents

Table S1. Electrochemical data for dppz ligands **A**-**C** and respective Ru(II) complexes **1A**-**3A**, **1B**, **2B** and **1C**-**3C**

Figure S1. High resolution ESI-MS spectrum of **1A**

Figure S2. High resolution ESI-MS spectrum of **2A**

Figure S3. High resolution ESI-MS spectrum of **3A**

Figure S4. High resolution ESI-MS spectrum of **1B**

Figure S5. High resolution ESI-MS spectrum of **2B**

Figure S6. High resolution ESI-MS spectrum of **1C**

Figure S7. High resolution ESI-MS spectrum of **2C**

Figure S8. High resolution ESI-MS spectrum of **3C**

Figure S9. ^{1}H NMR spectrum of **1A** recorded in DMSO-*d*^{6}

Figure S10. ^{13}C NMR spectrum of **1A** recorded in DMSO-*d*^{6}

Figure S11. ^{1}H NMR spectrum of **2A** recorded in DMSO-*d*^{6}

Figure S12. ^{13}C NMR spectrum of **2A** recorded in DMSO-*d*^{6}

Figure S13. ^{1}H NMR spectrum of **3A** recorded in DMSO-*d*^{6}

Figure S14. ^{13}C NMR spectrum of **3A** recorded in DMSO-*d*^{6}

Figure S15. ^{1}H NMR spectrum of **1B** recorded in DMSO-*d*^{6}

Figure S16. ^{13}C NMR spectrum of **1B** recorded in DMSO-*d*^{6}

Figure S17. ^{1}H NMR spectrum of **2B** recorded in DMSO-*d*^{6}

Figure S18. ^{13}C NMR spectrum of **2B** recorded in DMSO-*d*^{6}

Figure S19. ^{1}H NMR spectrum of **1C** recorded in DMSO-*d*^{6}

Figure S20. ^{13}C NMR spectrum of **1C** recorded in DMSO-*d*^{6}

Figure S21. ^{1}H NMR spectrum of **2C** recorded in DMSO-*d*^{6}

Figure S22. ^{13}C NMR spectrum of **2C** recorded in DMSO-*d*^{6}

Figure S23. ^{1}H NMR spectrum of **3C** recorded in DMSO-*d*^{6}

Figure S24. ^{13}C NMR spectrum of **3C** recorded in DMSO-*d*^{6}

Figure S25. ^{1}H NMR study on the stability of **1A** in DMSO-*d*^{6} for 72 h.

Figure S26. ^{1}H NMR study on the stability of **2A** in DMSO-*d*^{6} for 72 h.

Figure S27. ^{1}H NMR study on the stability of **3A** in DMSO-*d*^{6} for 72 h.

Figure S28. ^{1}H NMR study on the stability of **1B** in DMSO-d^6 for 72 h.

Figure S29. ^{1}H NMR study on the stability of **2B** in DMSO-d^6 for 72 h.

Figure S30. ^{1}H NMR study on the stability of **1C** in DMSO-d^6 for 72 h.

Figure S31. ^{1}H NMR study on the stability of **2C** in DMSO-d^6 for 72 h.

Figure S32. ^{1}H NMR study on the stability of **3C** in DMSO-d^6 for 72 h.

Figure S33. Stability of **1A** in 1% DMSO in PBS (A) and cell culture media (DMEM containing 10% FBS and 1% of Penicillin-Streptomycin (10,000 U/mL))/ H_2O in ratio 1:9 at 0, 24 and 72h.

Figure S34. Stability of **2A** in 1% DMSO in PBS (A) and cell culture media (DMEM containing 10% FBS and 1% of Penicillin-Streptomycin (10,000 U/mL))/ H_2O in ratio 1:9 at 0, 24 and 72h.

Figure S35. Stability of **3A** in 1% DMSO in PBS (A) and cell culture media (DMEM containing 10% FBS and 1% of Penicillin-Streptomycin (10,000 U/mL))/ H_2O in ratio 1:9 at 0, 24 and 72h.

Figure S36. Stability of **1B** in 1% DMSO in PBS (A) and cell culture media (DMEM containing 10% FBS and 1% of Penicillin-Streptomycin (10,000 U/mL))/ H_2O in ratio 1:9 at 0, 24 and 72h.

Figure S37. Stability of **2B** in 1% DMSO in PBS (A) and cell culture media (DMEM containing 10% FBS and 1% of Penicillin-Streptomycin (10,000 U/mL))/ H_2O in ratio 1:9 at 0, 24 and 72h.

Figure S38. Stability of **1C** in 1% DMSO in PBS (A) and cell culture media (DMEM containing 10% FBS and 1% of Penicillin-Streptomycin (10,000 U/mL))/ H_2O in ratio 1:9 at 0, 24 and 72h.

Figure S39. Stability of **2C** in 1% DMSO in PBS (A) and cell culture media (DMEM containing 10% FBS and 1% of Penicillin-Streptomycin (10,000 U/mL))/ H_2O in ratio 1:9 at 0, 24 and 72h.

Figure S40. Stability of **3C** in 1% DMSO in PBS (A) and cell culture media (DMEM containing 10% FBS and 1% of Penicillin-Streptomycin (10,000 U/mL))/ H_2O in ratio 1:9 at 0, 24 and 72h.

Figure S41. Flow cytometry analysis of intracellular ROS generation by **3A** and **A** by measuring the fluorescence intensity of DCF in FL-1 channel (excitation and emission wavelengths of 498 and 522 nm, respectively) in HCT116 cancer cells.

Figure S42. Concentration-effect curves for **1A**-**3A**, **1B**, **2B** and **1C**-**3C** in MDA-MB-231 and HCT116 cells lines upon 72 h exposure.

Figure S43. H&E-stained tumor sections in a Ru complex **3A**-treated group.

Figure S44. H&E-stained tumor sections in a vehicle-treated group.

Figure S45. H&E-stained tumor sections in a ligand **A**-treated group.

Figure S46. H&E-stained kidney and liver sections in a vehicle- and ligand **A**-treated groups.

Table S1. Electrochemical data for dppz ligands **A**-**C** and respective Ru(II) complexes **1A**-**3A**, **1B**, **2B** and **1C**-**3C** in DMSO-based electrolyte solution (*n*-Bu_4NClO_4, 0.1 M) recorded with a glassy-carbon working electrode at scan rate of 50 mV s^{-1} and referenced to a Ag/AgCl reference electrode.

Compound	Reduction, E_{red}	Oxidation, E_{ox}
A	-0.47	0.91, 0.99
B	-0.37, -0.30	0.91, 0.99
C	-0.33, -0.28	0.88, 0.99
1A	-0.45	1.15
2A	-0.38	1.14
3A	-0.47	1.23
1B	-0.33, -0.55	1.15
2B	-0.29, -0.55	-
1C	-0.35, -0.51, -0.71	1.12
2C	-0.36, -0.53, -0.77	1.15
3C	-0.43, -0.61, -0.77	1.19

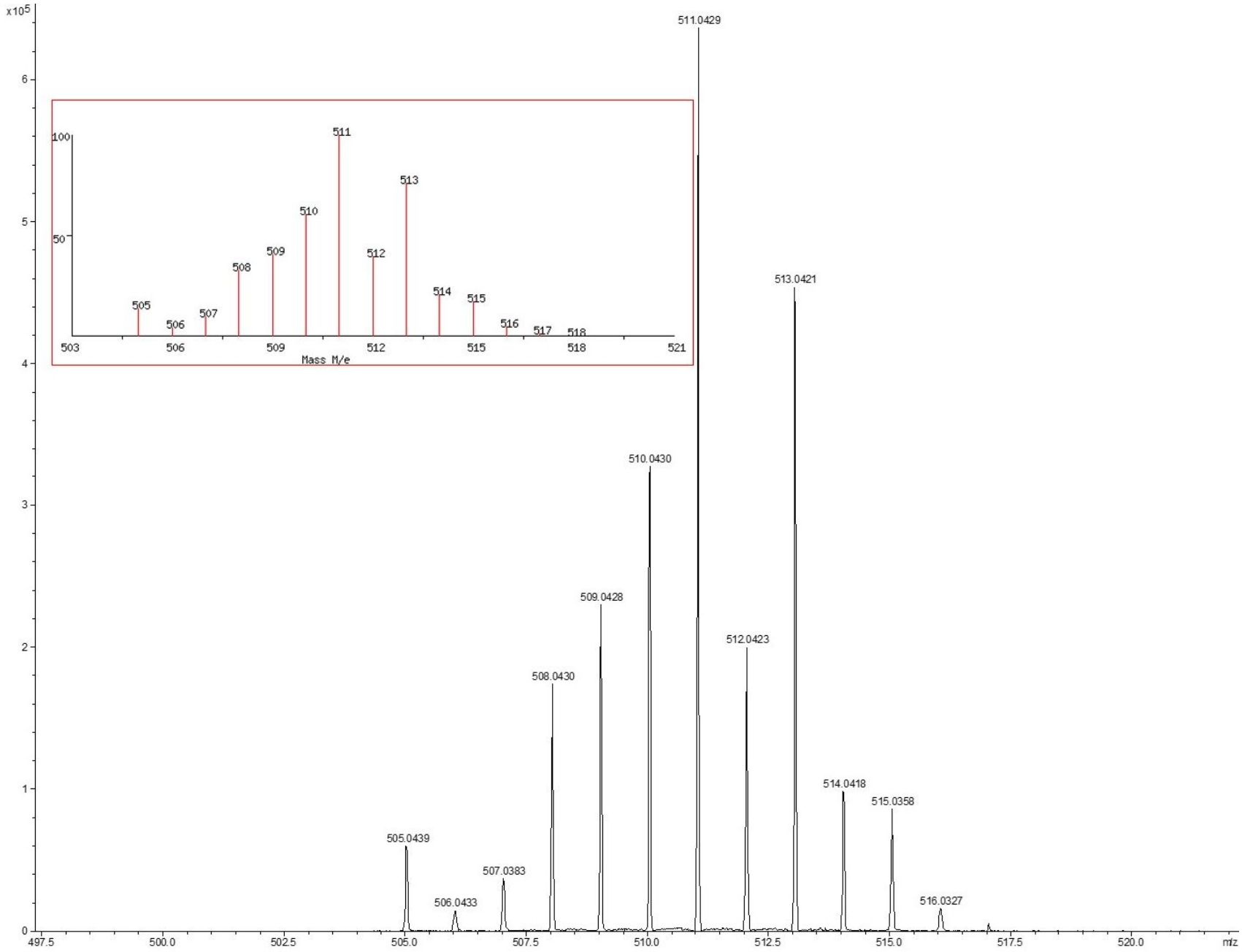
x10^5
511.0429
513.0421
510.0430
509.0428
512.0423
508.0430
514.0418
515.0358
505.0439
507.0383
506.0433
516.0327
m/z
Mass M/e
100
50

Figure S1. High resolution ESI-MS spectrum of **1A**.

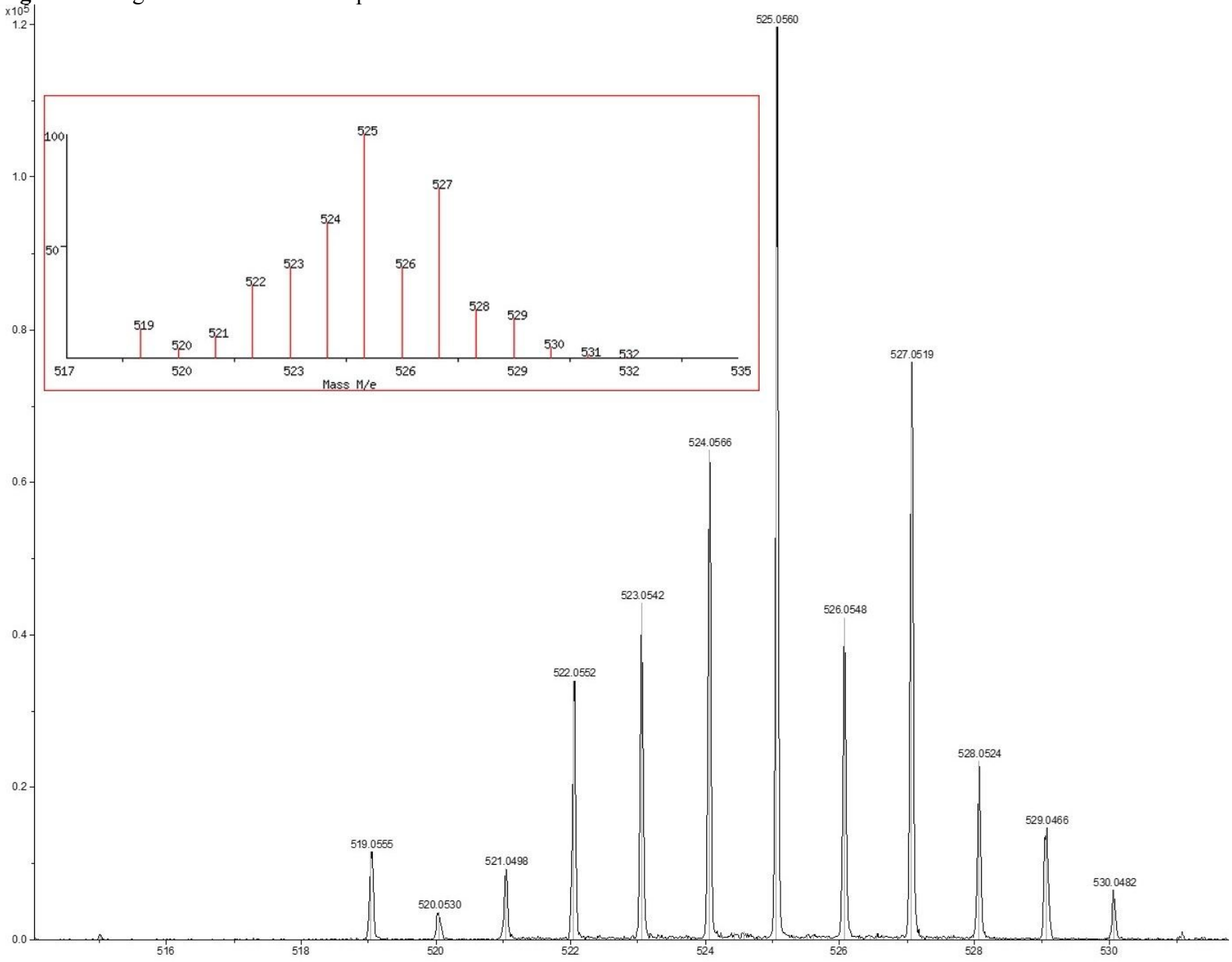

Figure S2. High resolution ESI-MS spectrum of **2A**.

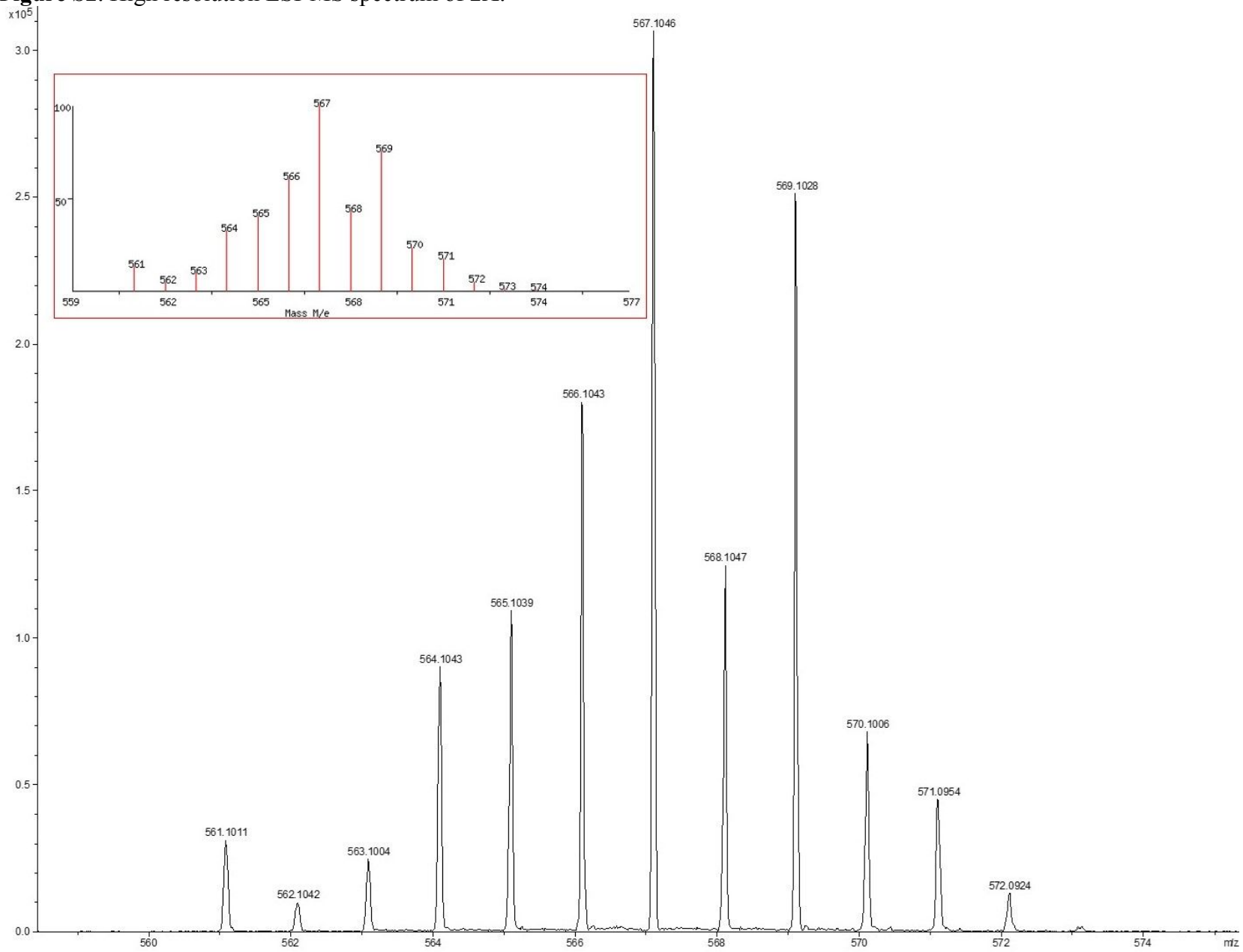

Figure S3. High resolution ESI-MS spectrum of **3A**.

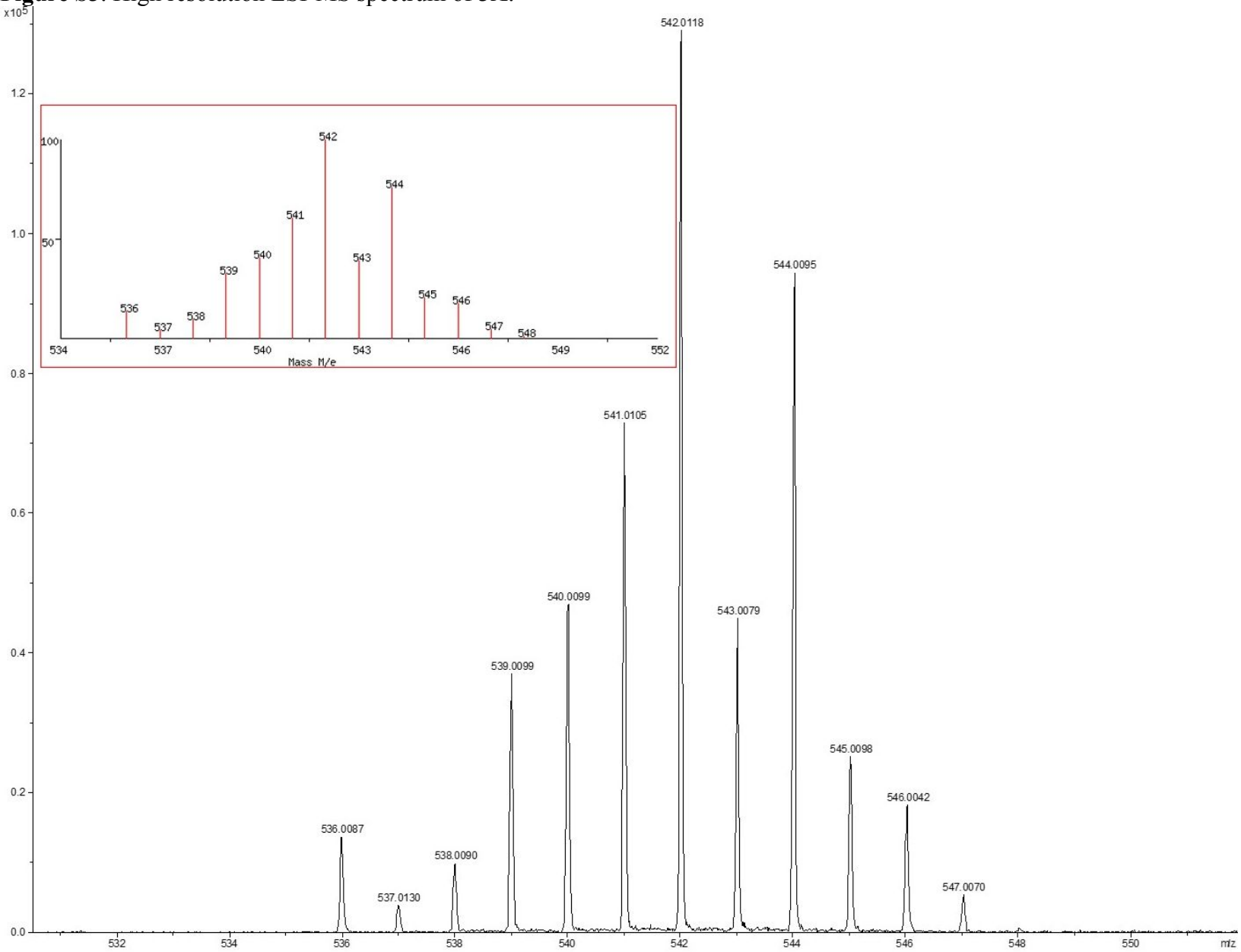

Figure S4. High resolution ESI-MS spectrum of **1B**.

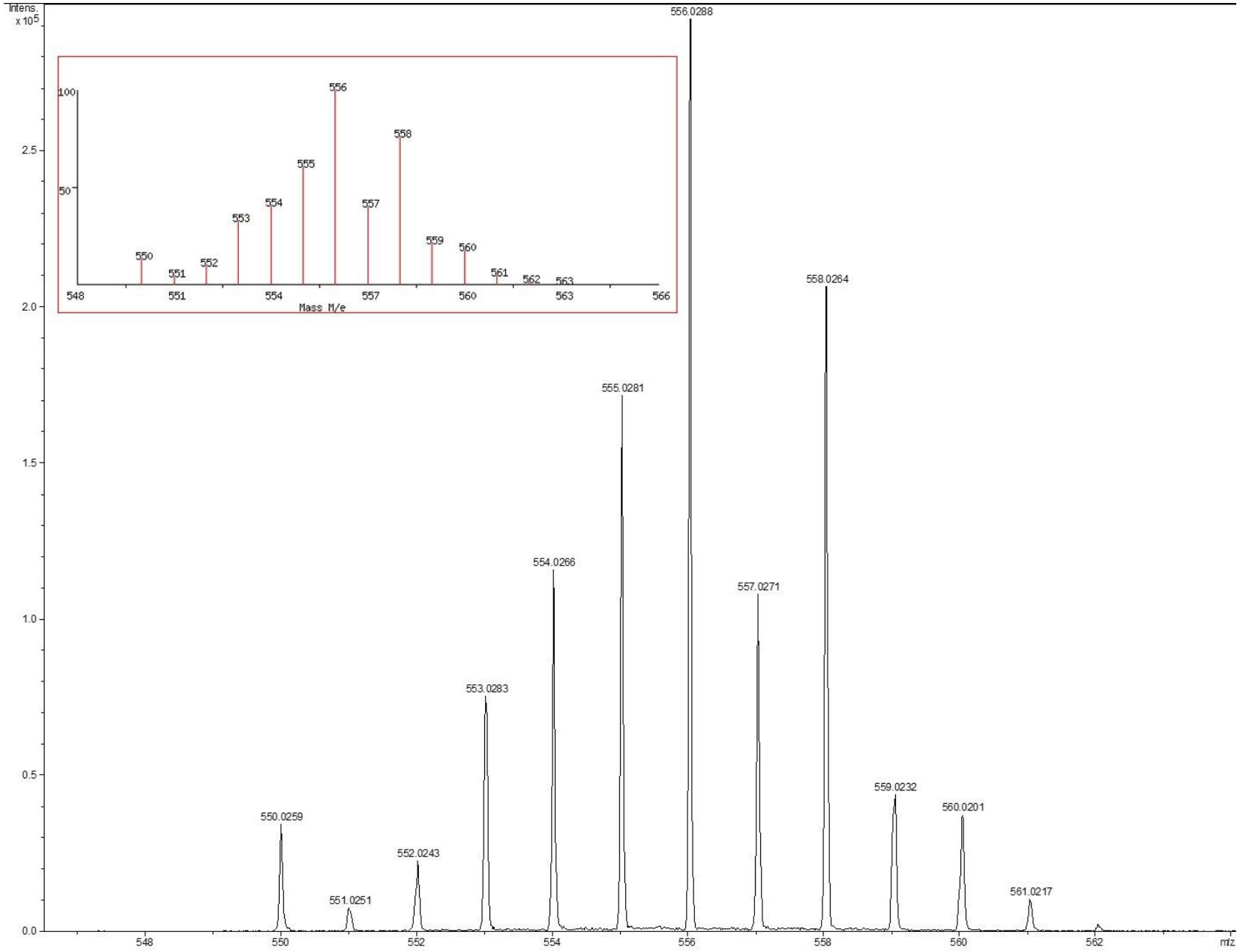

Figure S5. High resolution ESI-MS spectrum of **2B**.

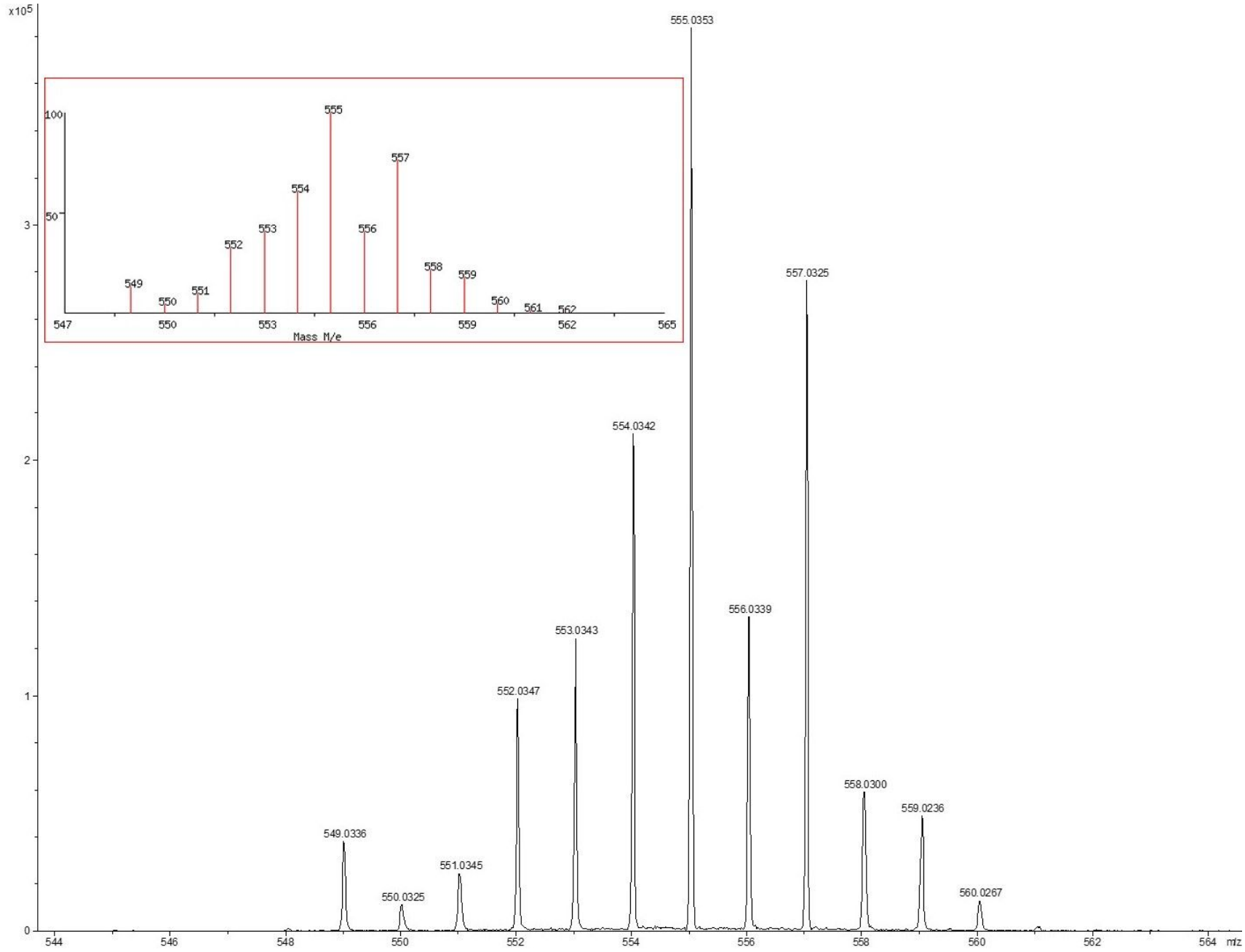
x10^5
555.0353
557.0325
554.0342
556.0339
553.0343
552.0347
558.0300
559.0236
549.0336
551.0345
550.0325
560.0267
m/z
Mass M/e

Figure S6. High resolution ESI-MS spectrum of **1C**.

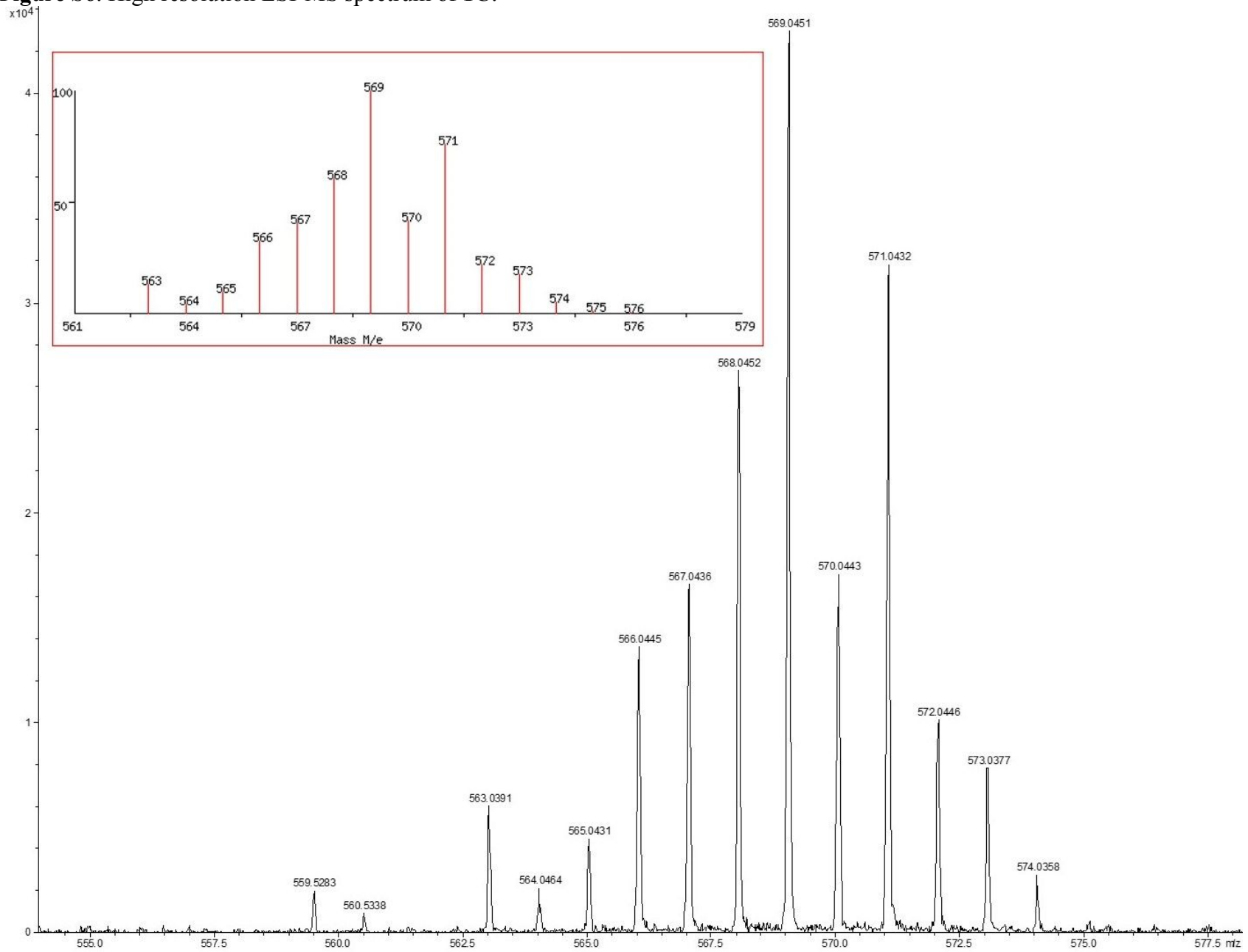

Figure S7. High resolution ESI-MS spectrum of **2C**.

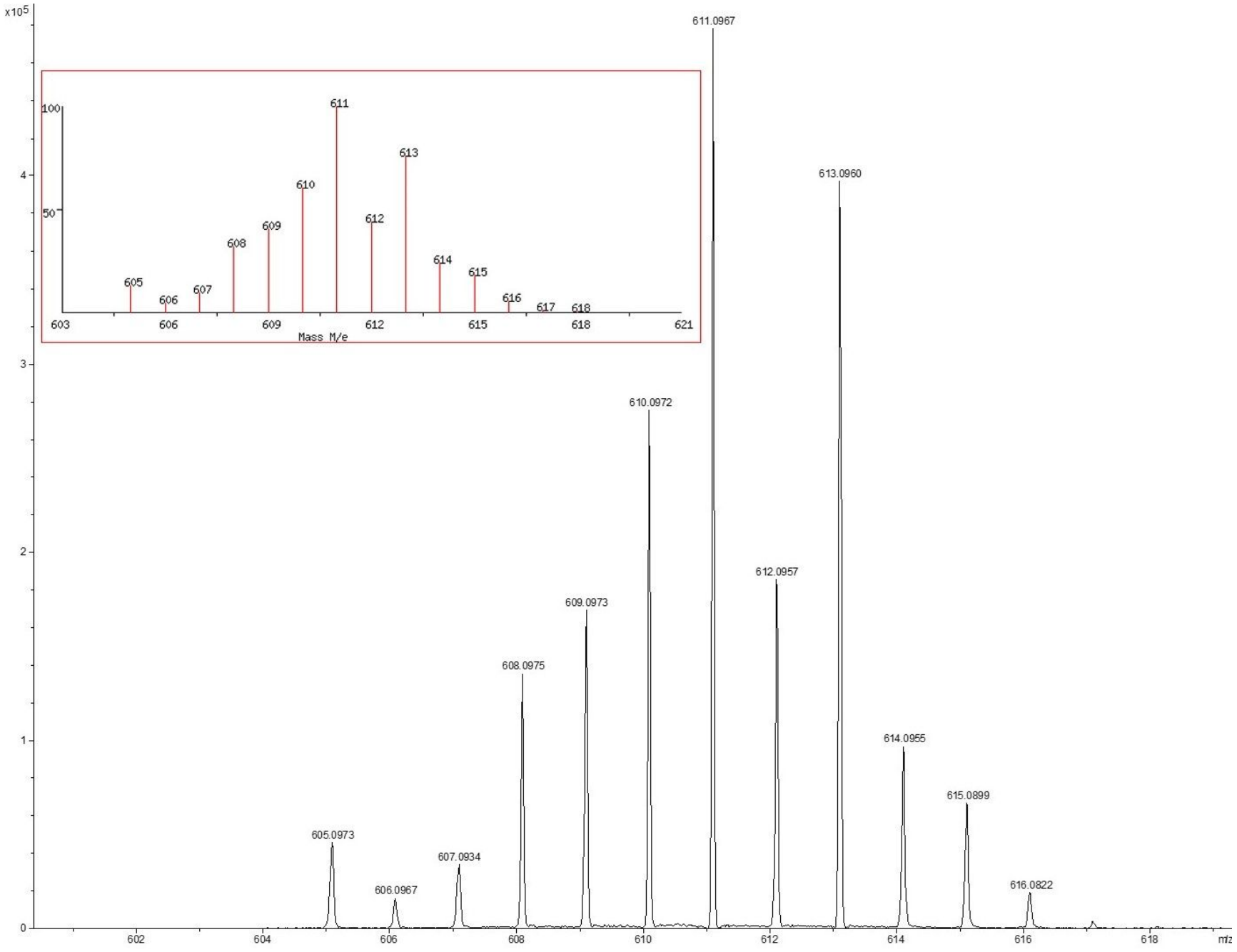
x10^5
611.0967
613.0960
610.0972
612.0957
609.0973
608.0975
614.0955
615.0899
605.0973
607.0934
606.0967
616.0822
0
1
2
3
4
602
604
606
608
610
612
614
616
618
m/z
100
50
611
613
610
612
609
608
614
615
605
606
607
616
617
618
603
606
609
612
615
618
621
Mass M/e

Figure S8. High resolution ESI-MS spectrum of **3C**.

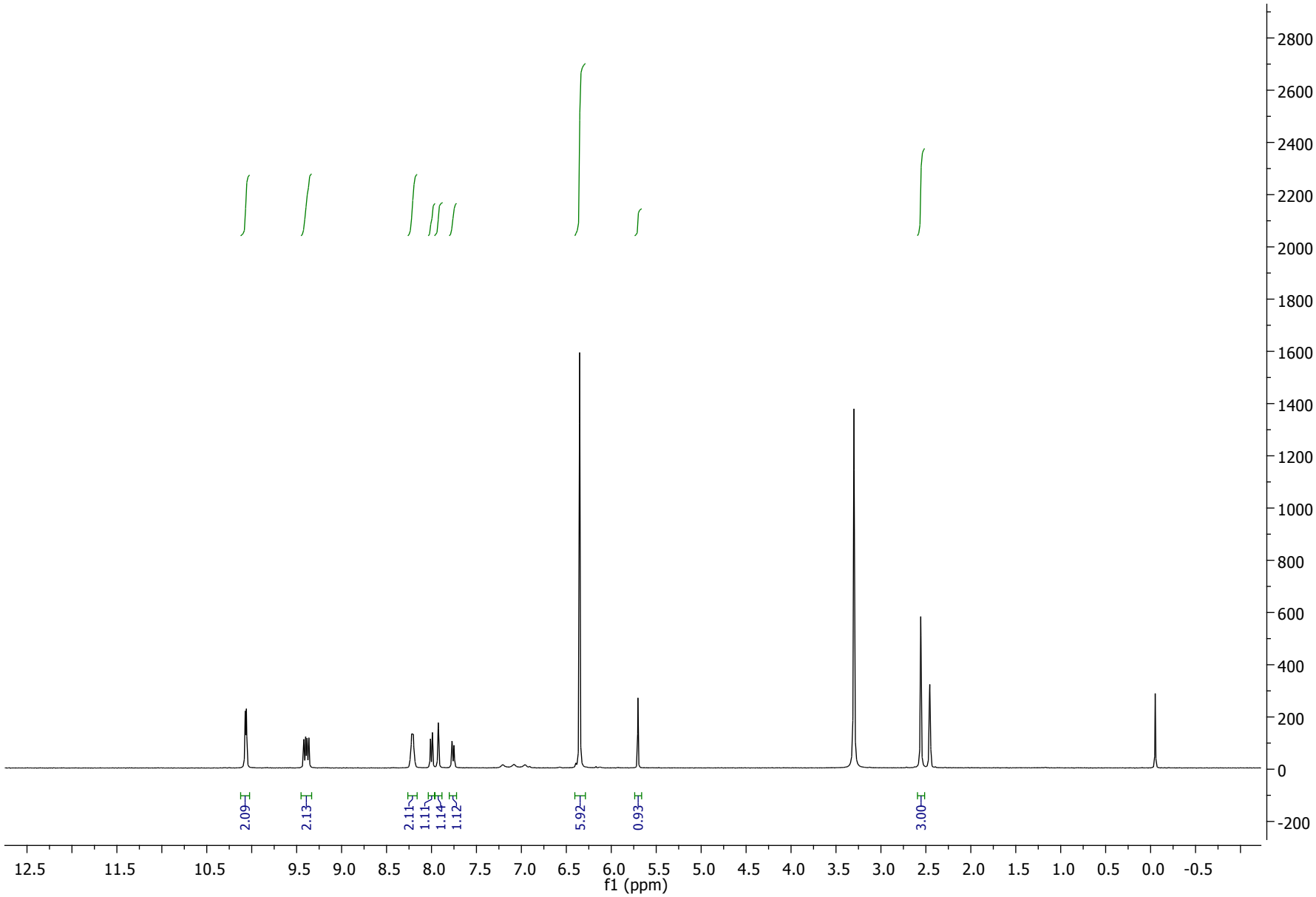

Figure S9. ^{1}H NMR spectrum of **1A** recorded in DMSO-d^{6}

.

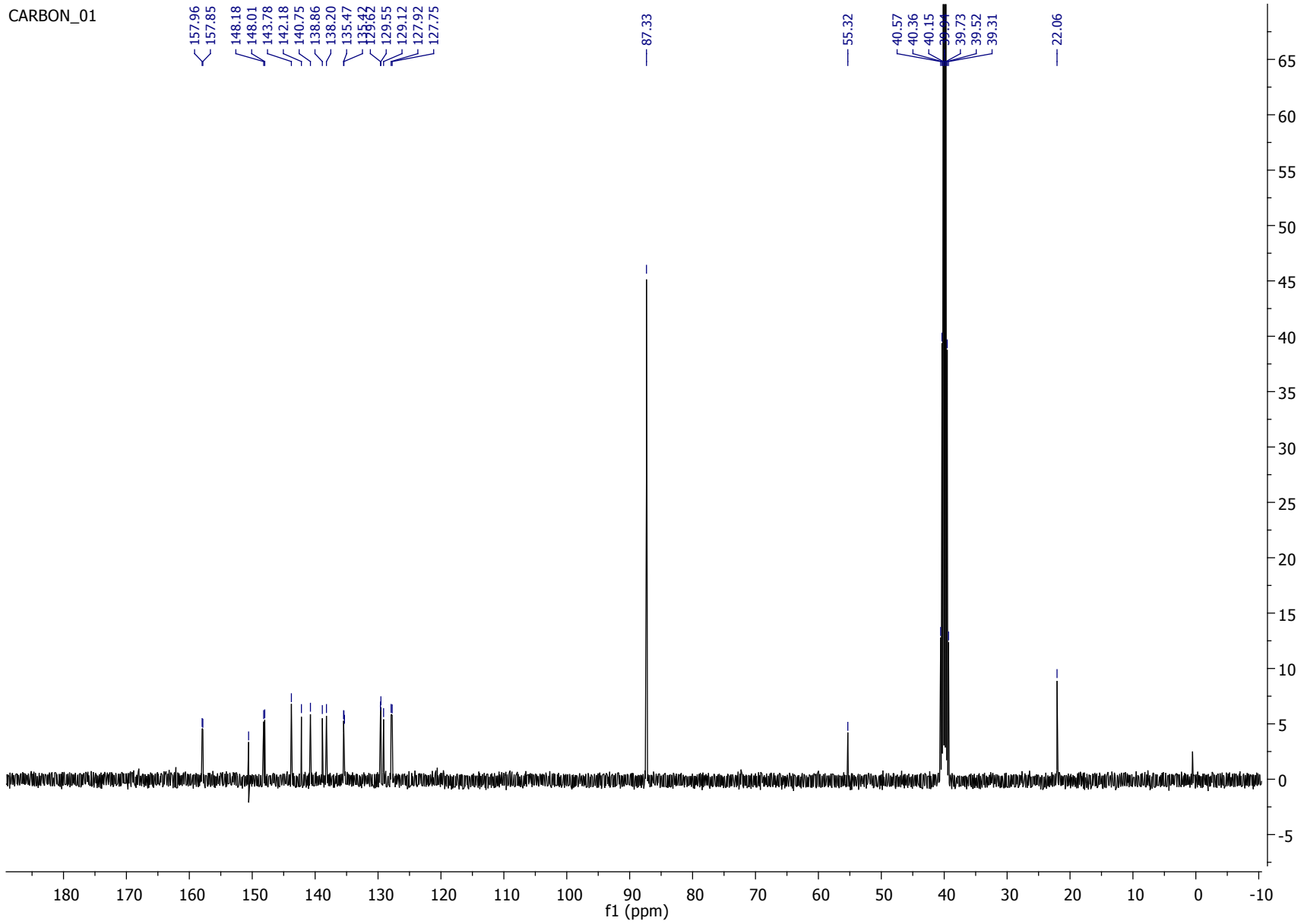

Figure S10. ^{13}C NMR spectrum of **1A** recorded in DMSO-d^6

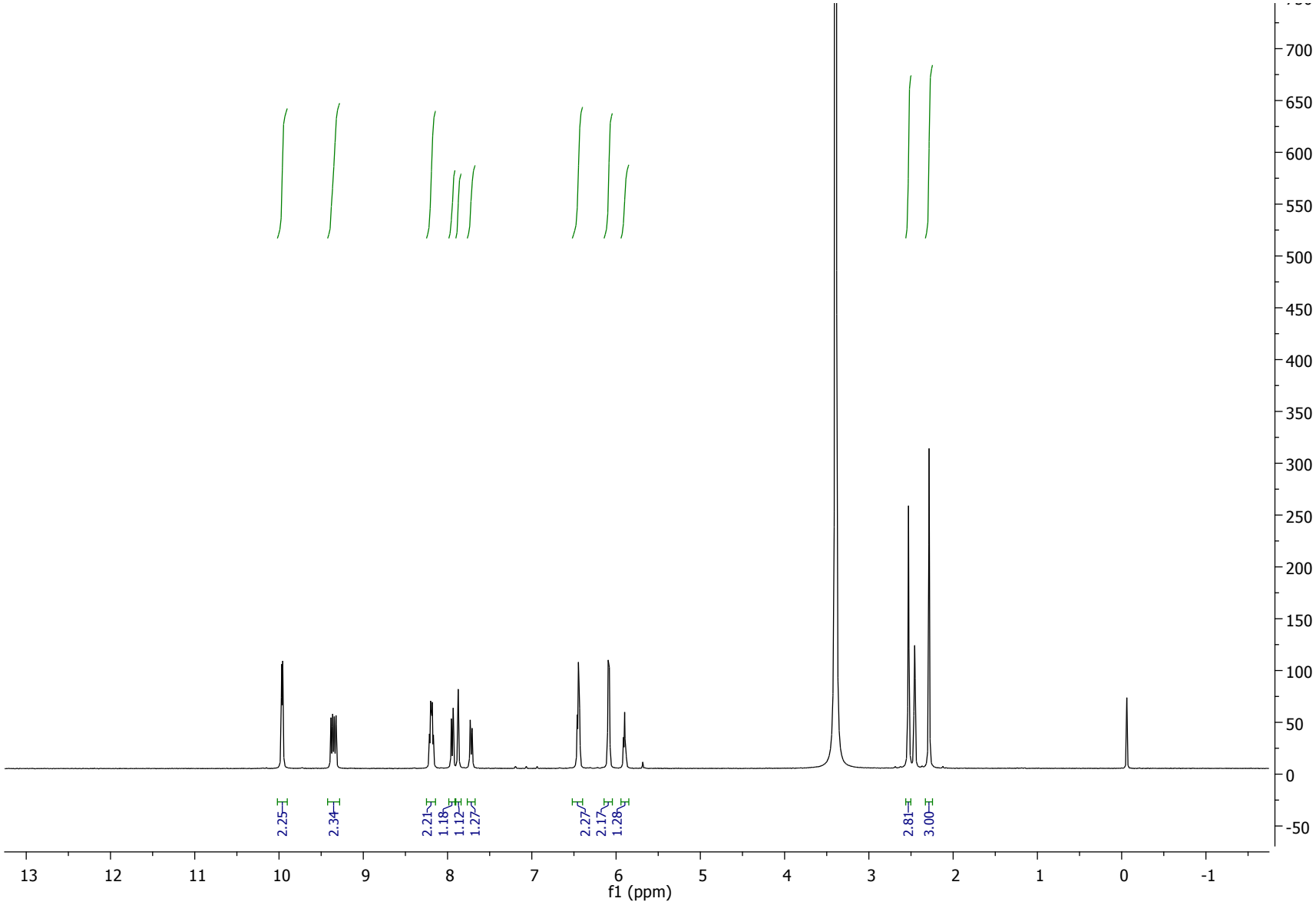

Figure S11. ^{1}H NMR spectrum of **2A** recorded in DMSO-d^{6}

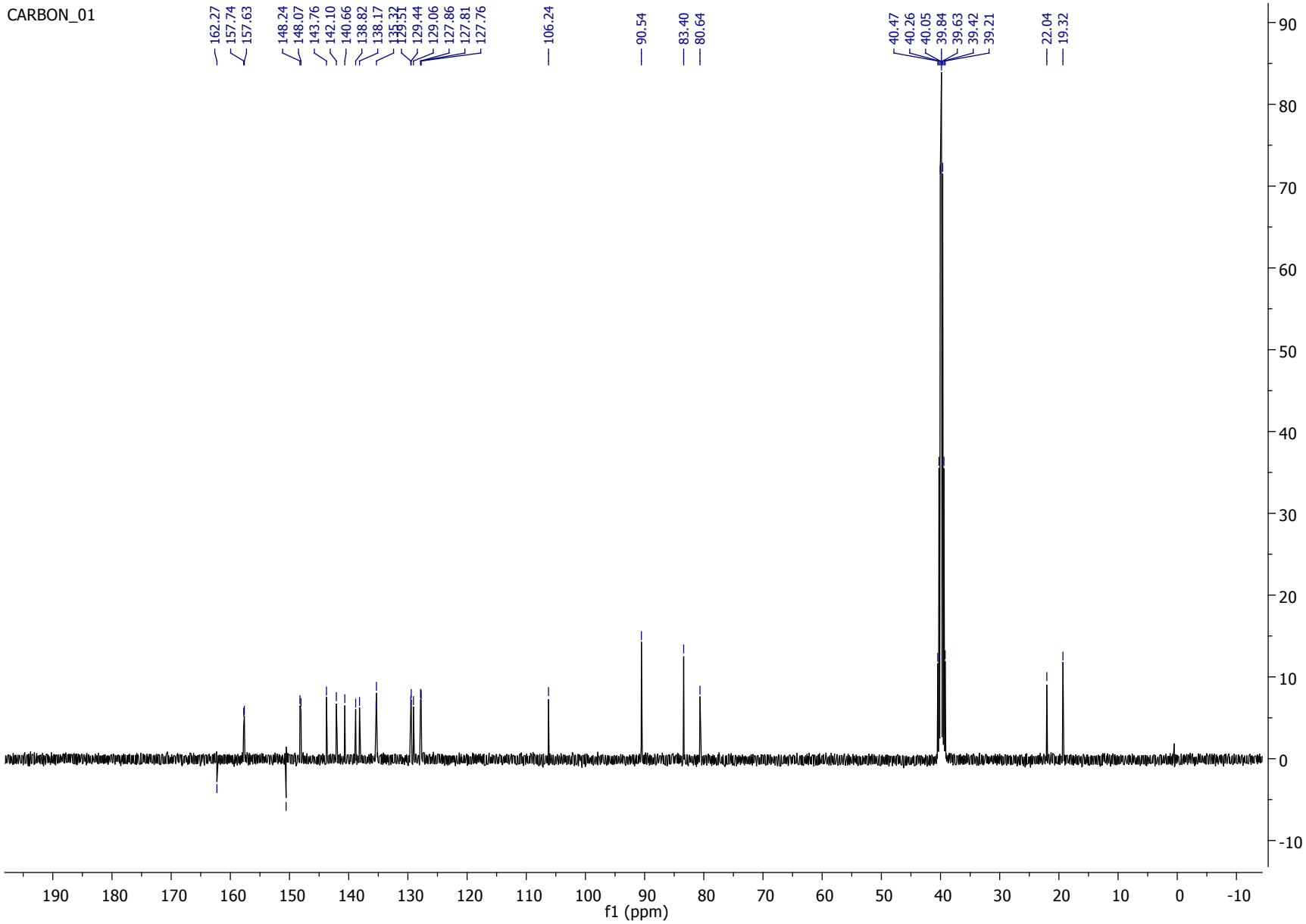
CARBON_01
162.27
157.74
157.63
148.24
148.07
143.76
142.10
140.66
138.82
138.17
135.32
129.51
129.44
129.06
127.86
127.81
127.76
106.24
90.54
83.40
80.64
40.47
40.26
40.05
39.84
39.63
39.42
39.21
22.04
19.32
f1 (ppm)

Figure S12. ^{13}C NMR spectrum of **2A** recorded in DMSO-d^6

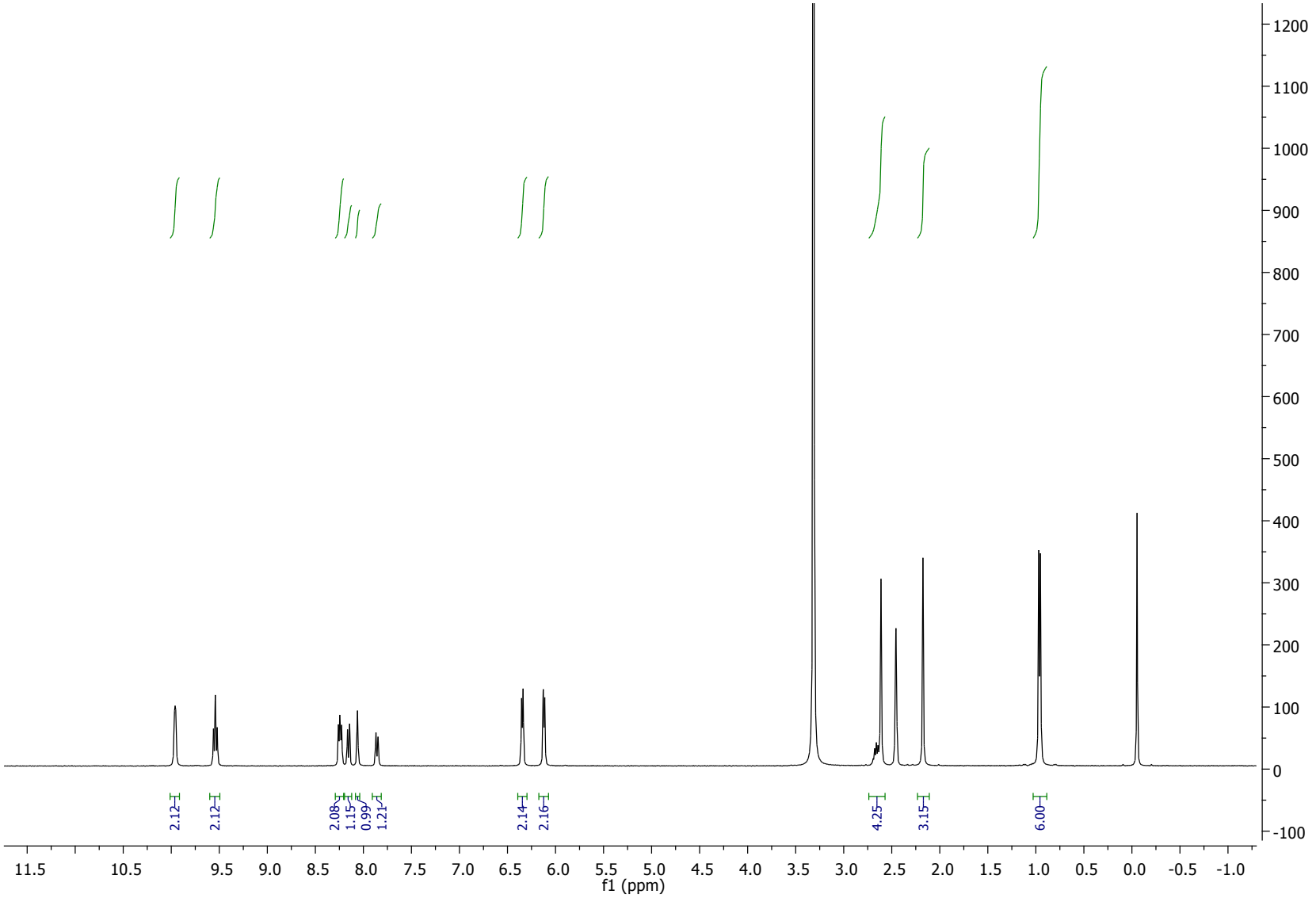

Figure S13. ^{1}H NMR spectrum of **3A** recorded in DMSO-d^{6}

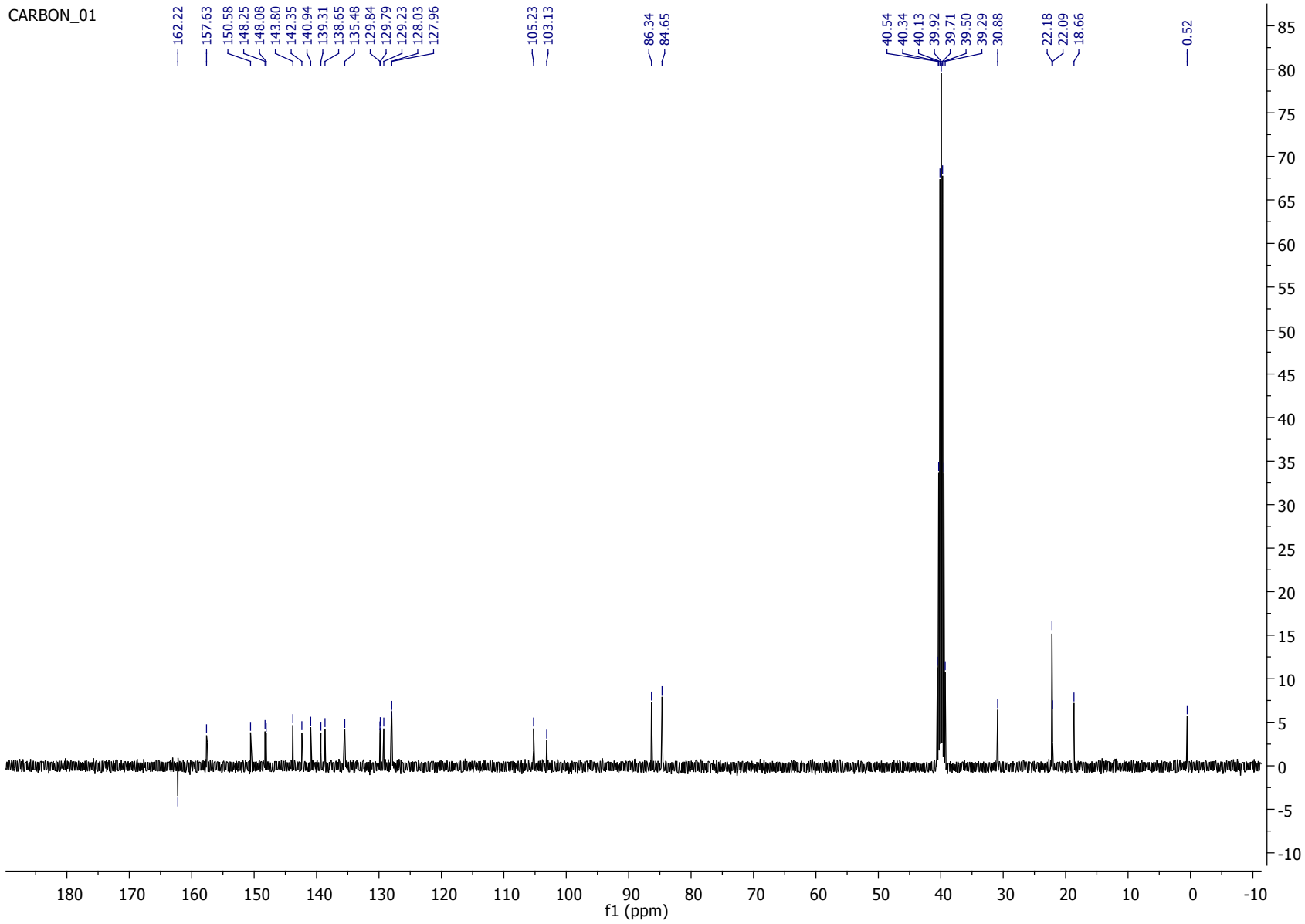

Figure S14. ^{13}C NMR spectrum of **3A** recorded in DMSO-d^6

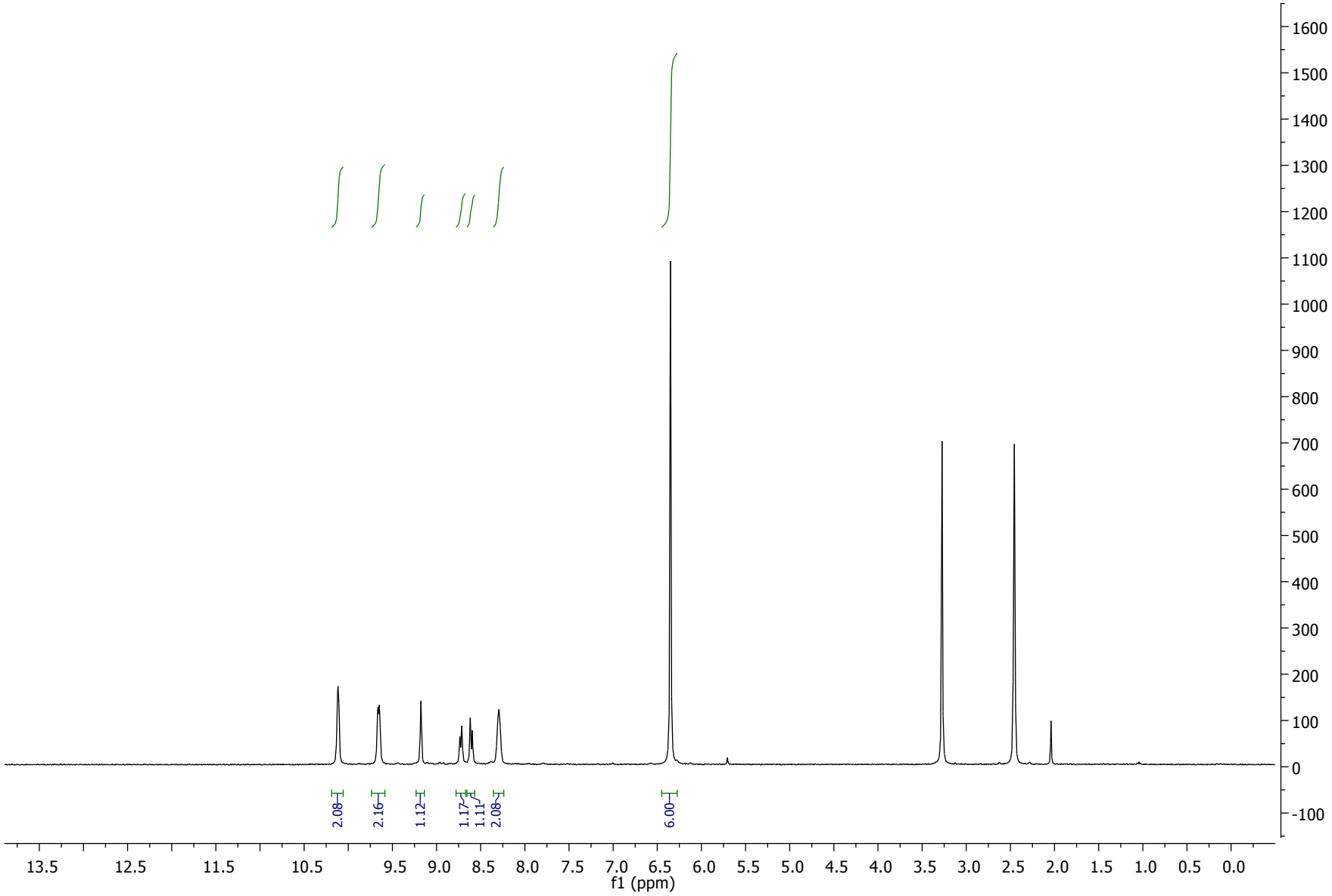

Figure S15. ^{1}H NMR spectrum of **1B** recorded in DMSO-d^{6}

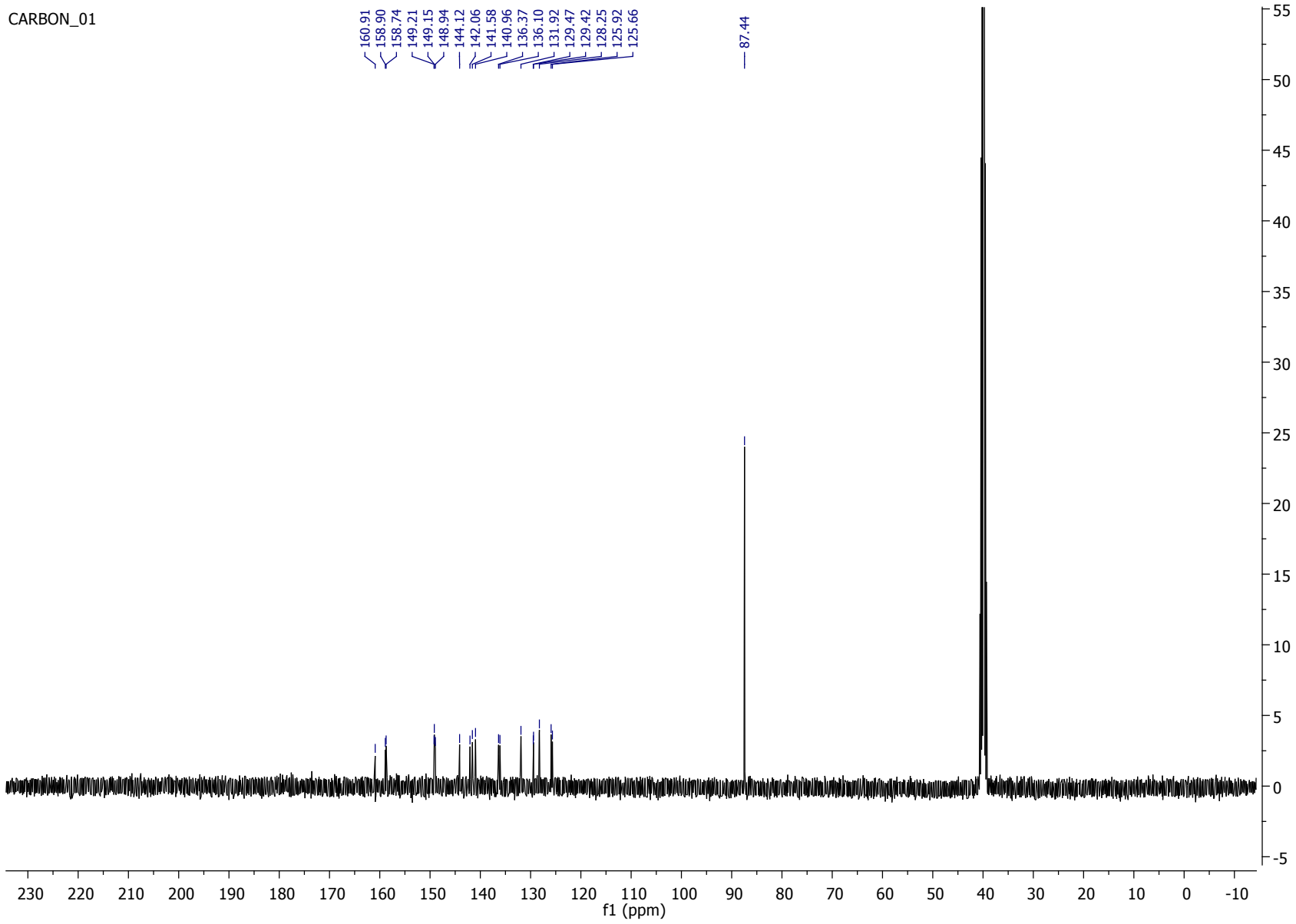
CARBON_01
160.91
158.90
158.74
149.21
149.15
148.94
144.12
142.06
141.58
140.96
136.37
136.10
131.92
129.47
129.42
128.25
125.92
125.66
87.44
f1 (ppm)

Figure S16. ^{13}C NMR spectrum of **1B** recorded in DMSO-d^6

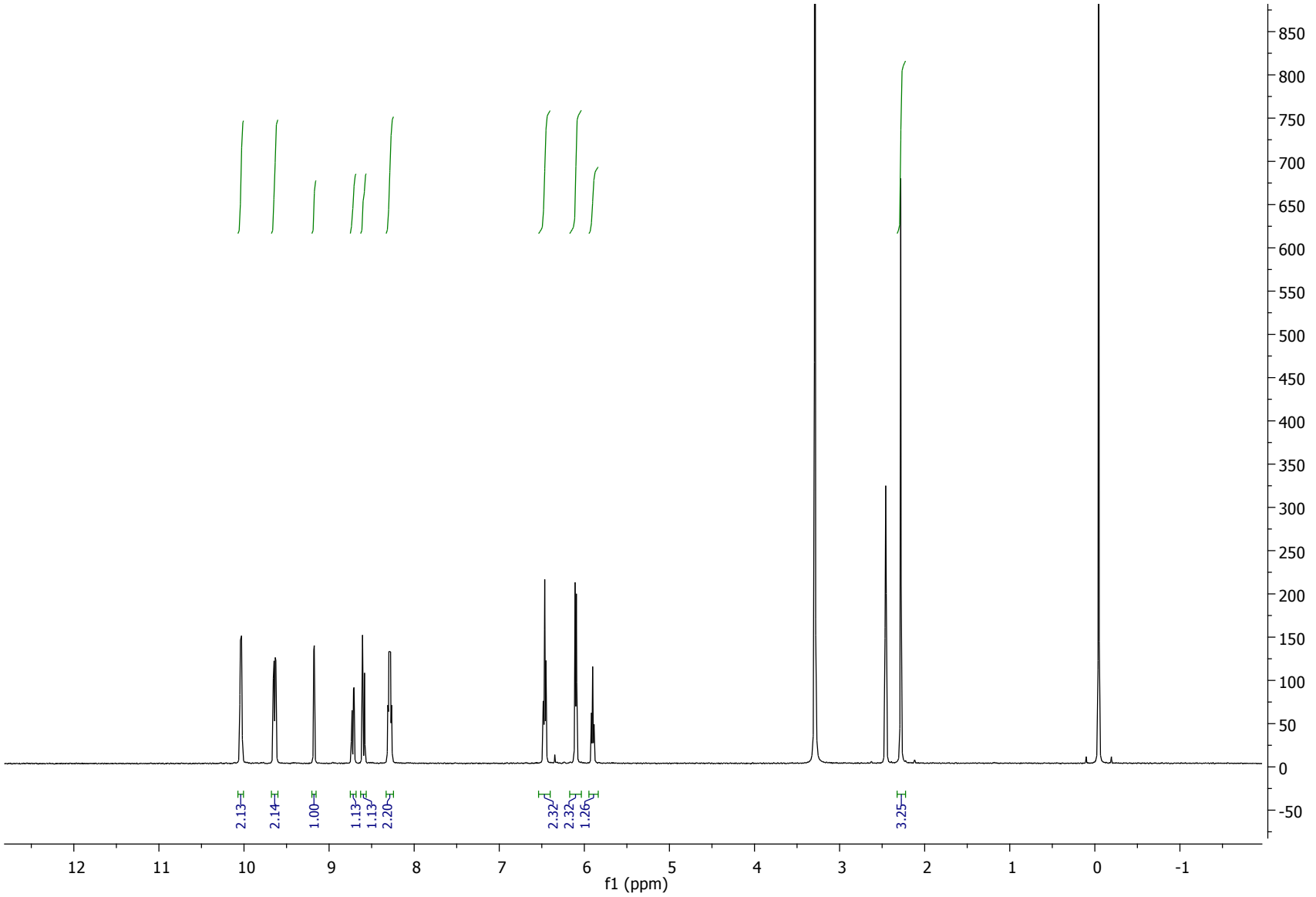

Figure S17. ^{1}H NMR spectrum of **2B** recorded in DMSO-d^{6}

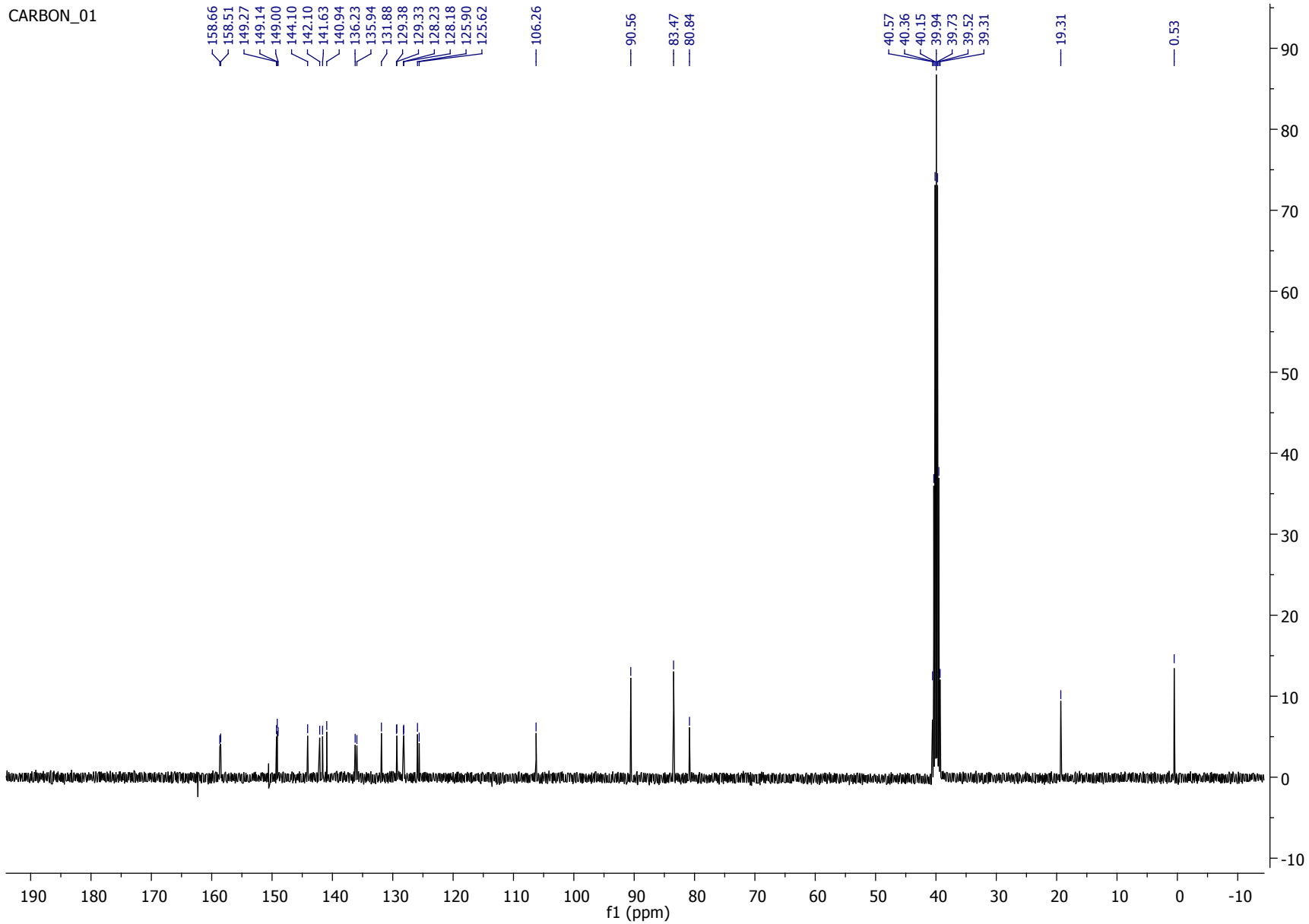

Figure S18. ^{13}C NMR spectrum of **2B** recorded in DMSO-d^6

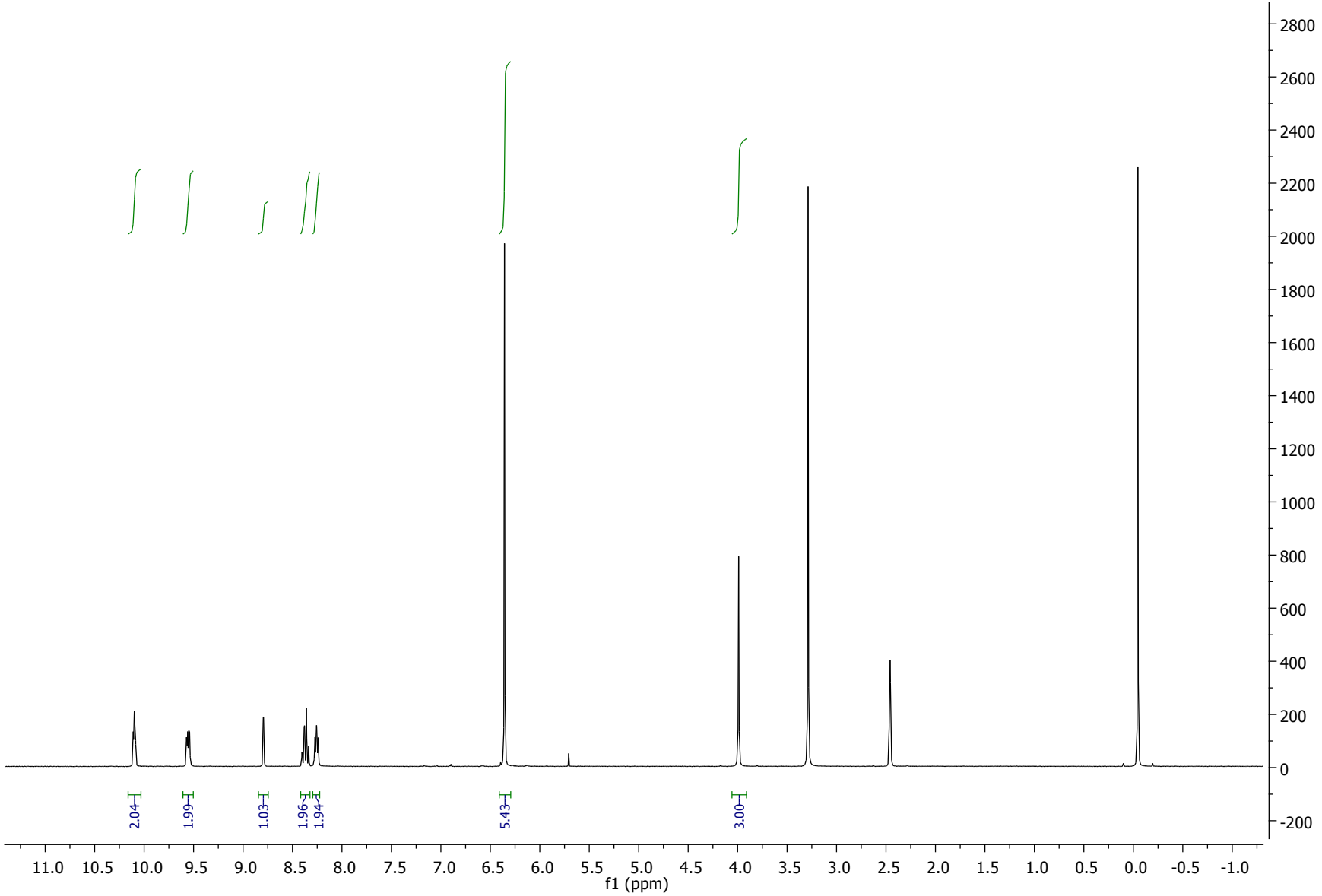
2.04
1.99
1.03
1.96
1.94
5.43
3.00
f1 (ppm)

Figure S19. [1]H NMR spectrum of **1C** recorded in DMSO-*d*[6]

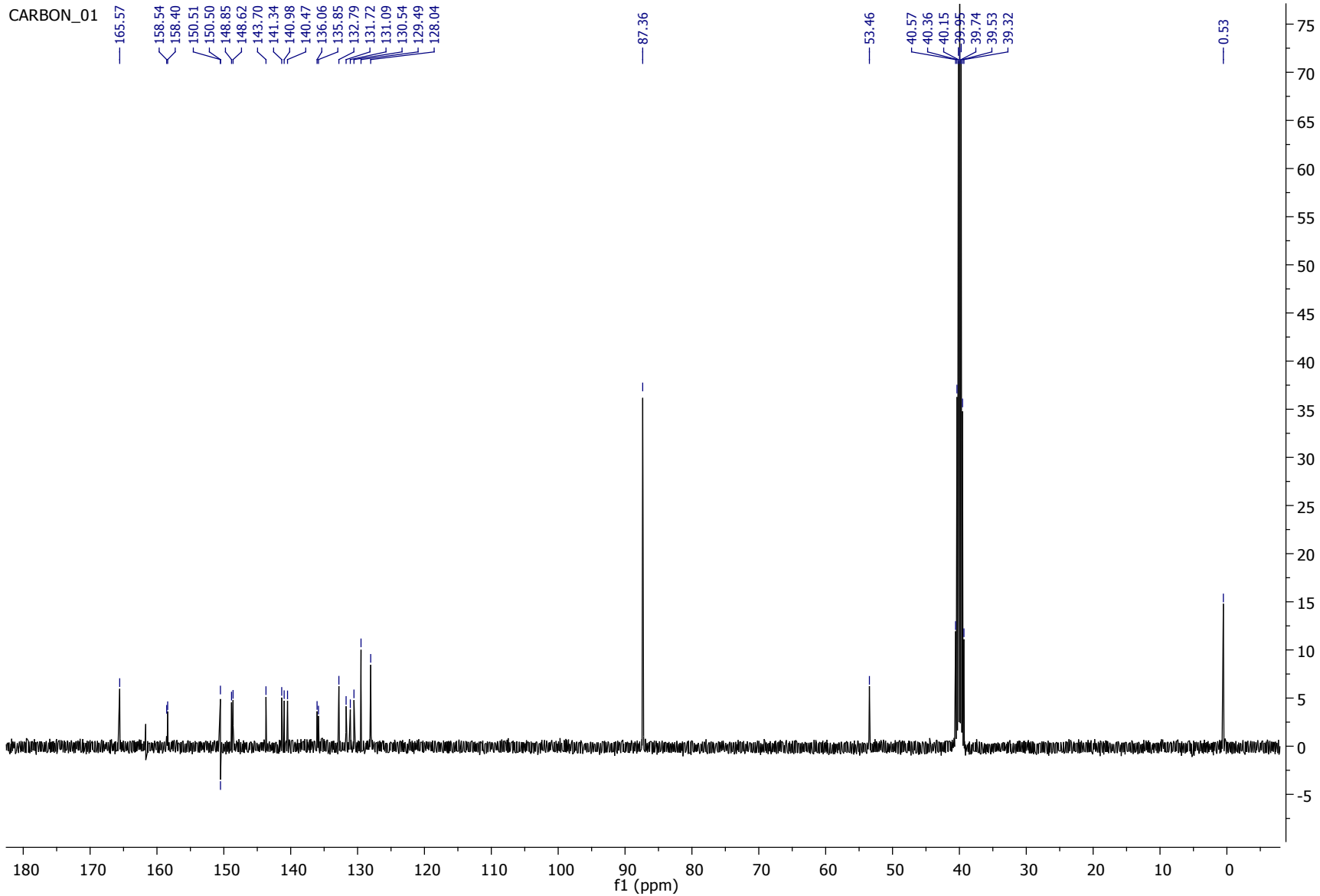

Figure S20. [13]C NMR spectrum of **1C** recorded in DMSO-*d*[6]

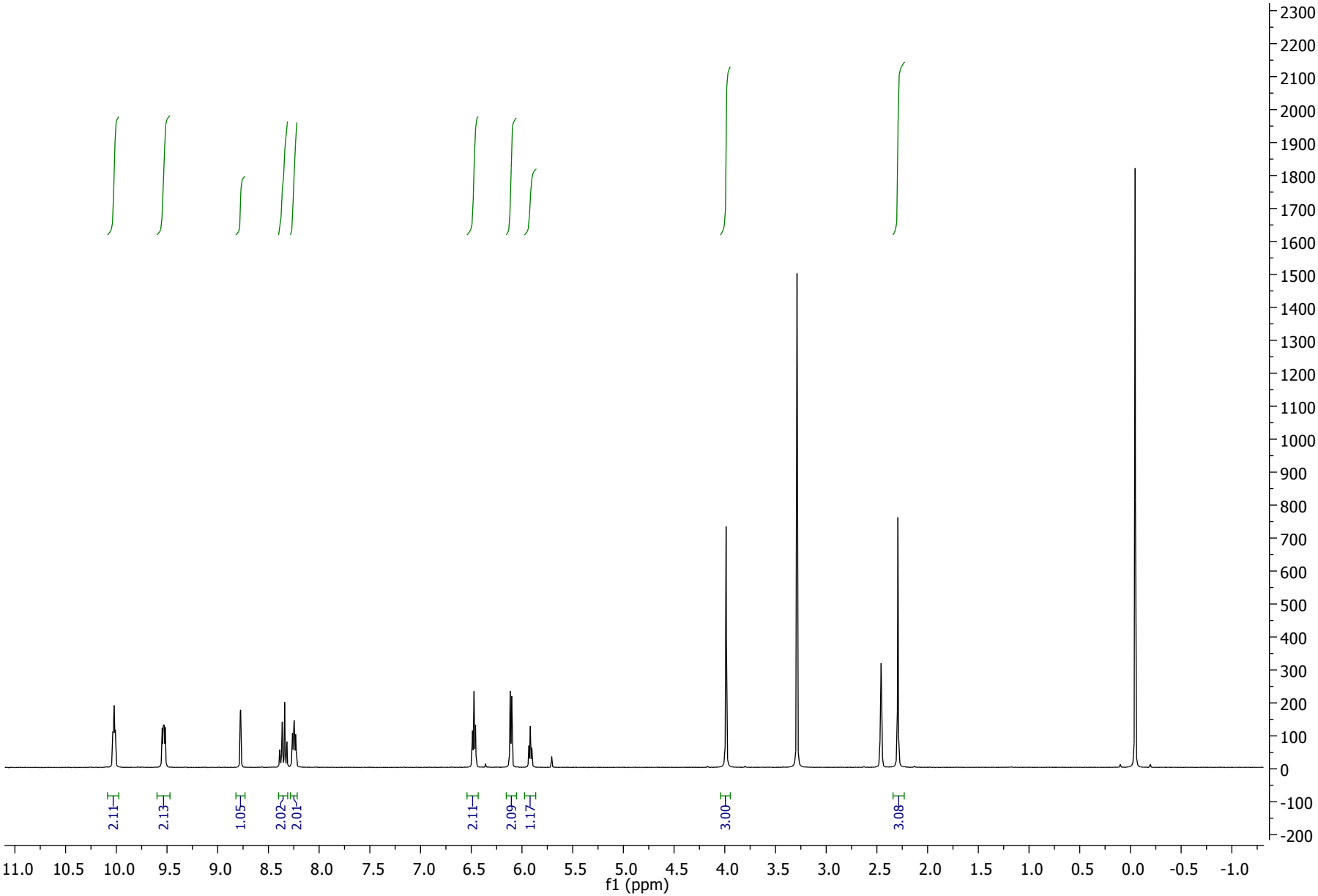
2.11
2.13
1.05
2.02
2.01
2.11
2.09
1.17
3.00
3.08
f1 (ppm)

Figure S21. ^{1}H NMR spectrum of **2C** recorded in DMSO-d^{6}

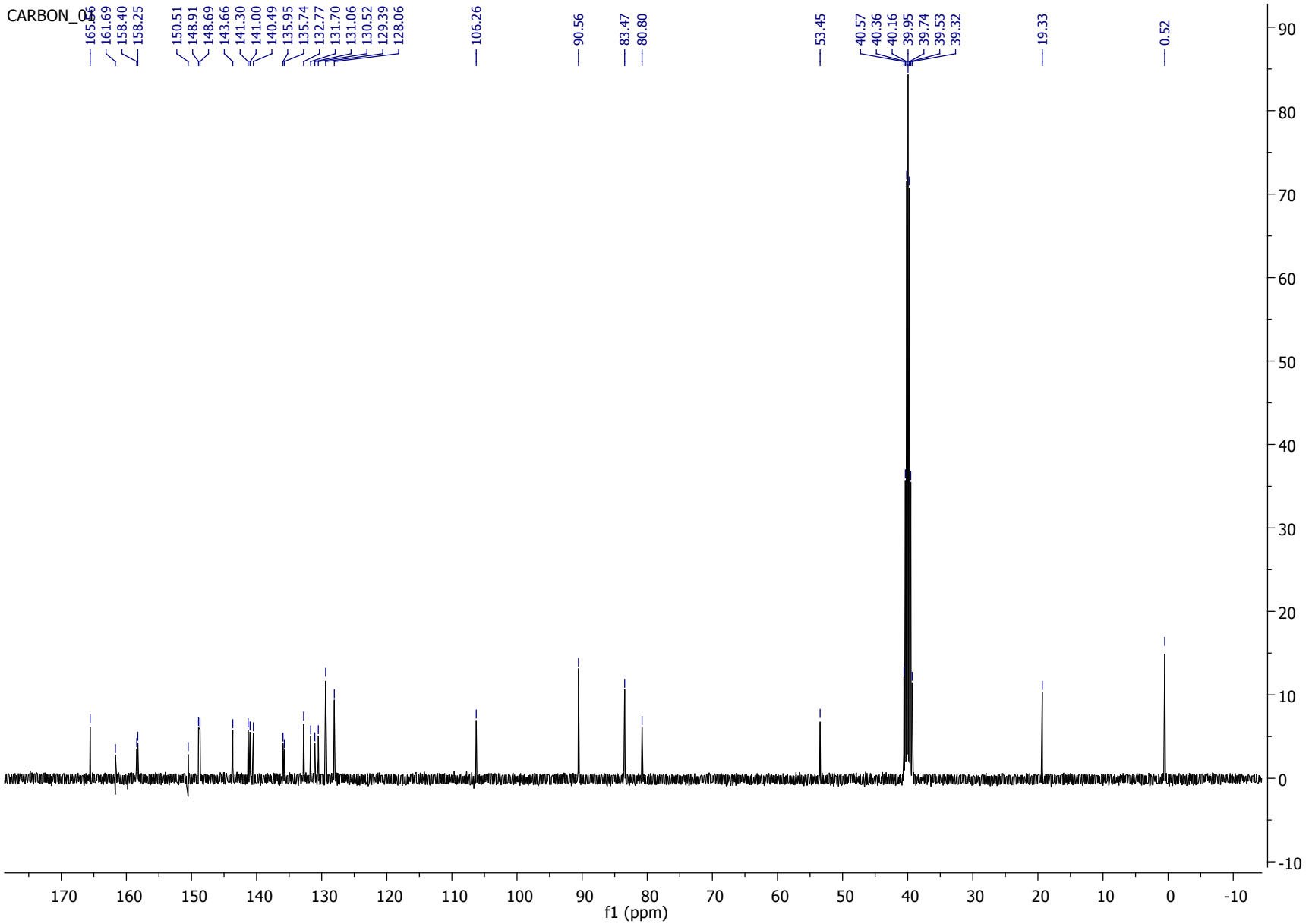

Figure S22. ^{13}C NMR spectrum of **2C** recorded in DMSO-d^6

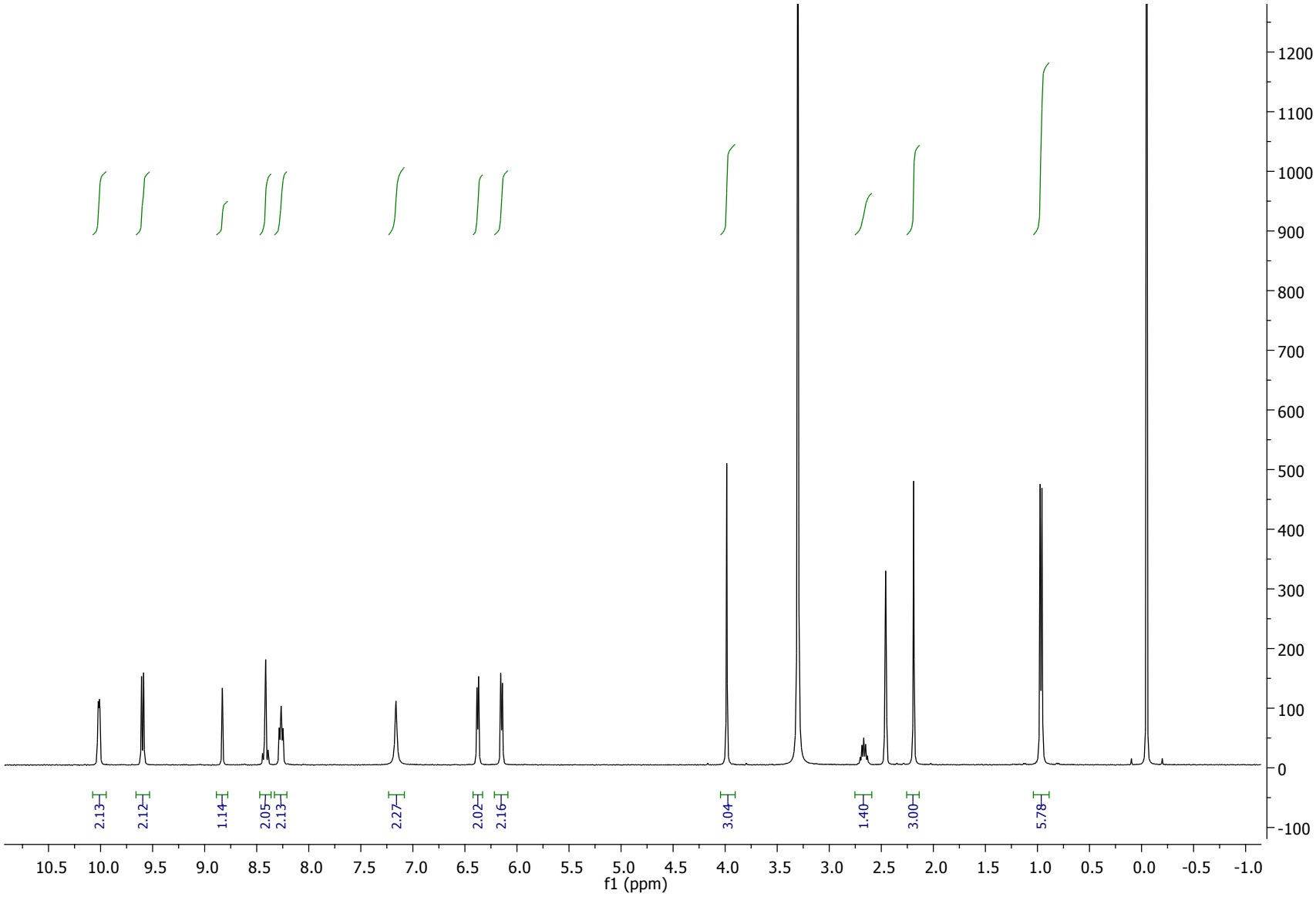
2.13
2.12
1.14
2.05
2.13
2.27
2.02
2.16
3.04
1.40
3.00
5.78
f1 (ppm)

Figure S23. ^{1}H NMR spectrum of **3C** recorded in DMSO-d^{6}

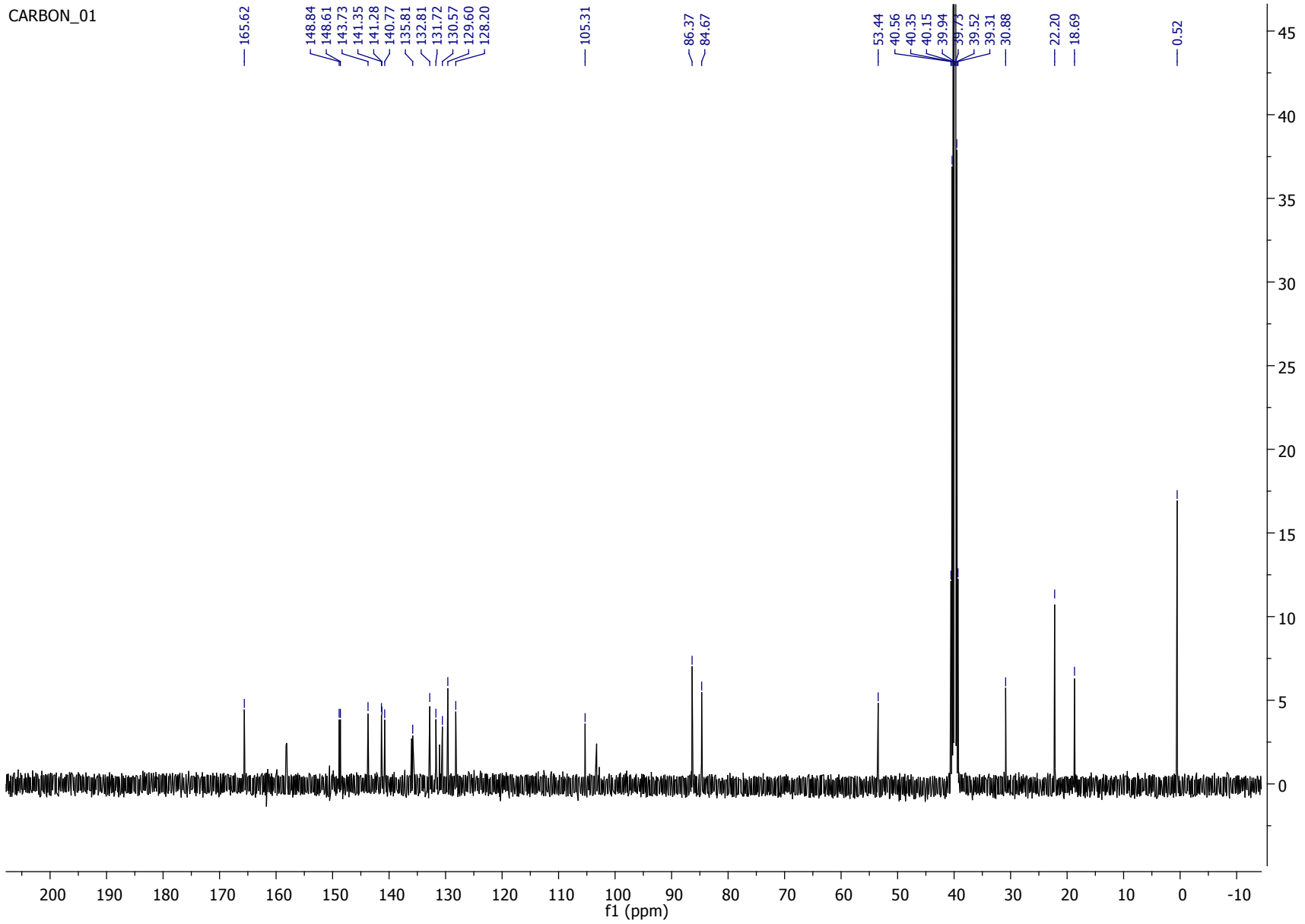

Figure S24. ^{13}C NMR spectrum of **3C** recorded in DMSO-d^6

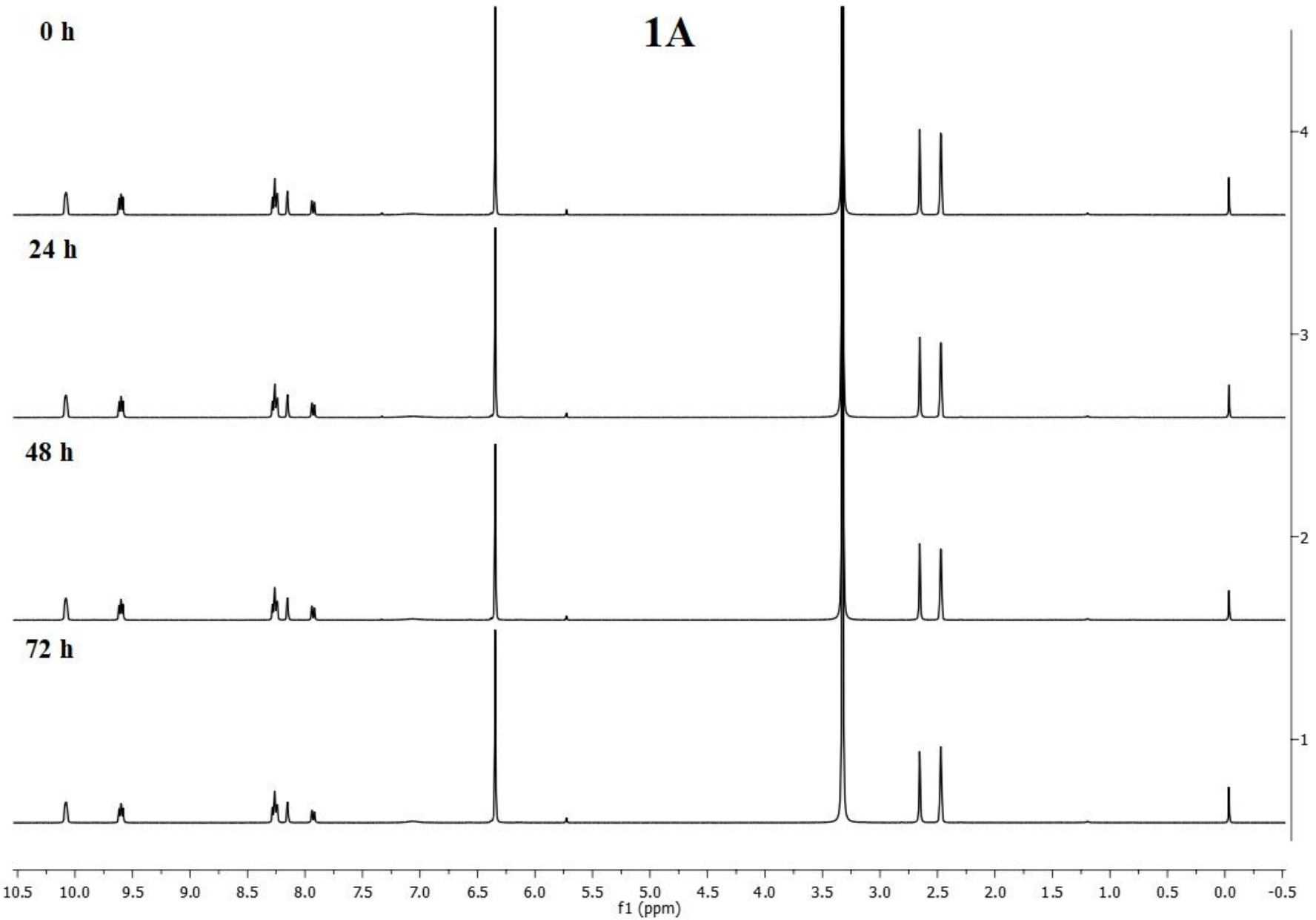
1A
0 h
24 h
48 h
72 h
4
3
2
1
10.5 10.0 9.5 9.0 8.5 8.0 7.5 7.0 6.5 6.0 5.5 5.0 4.5 4.0 3.5 3.0 2.5 2.0 1.5 1.0 0.5 0.0 -0.5
f1 (ppm)

Figure S25. ^{1}H NMR study on the stability of **1A** in DMSO-d^{6} for 72 h.

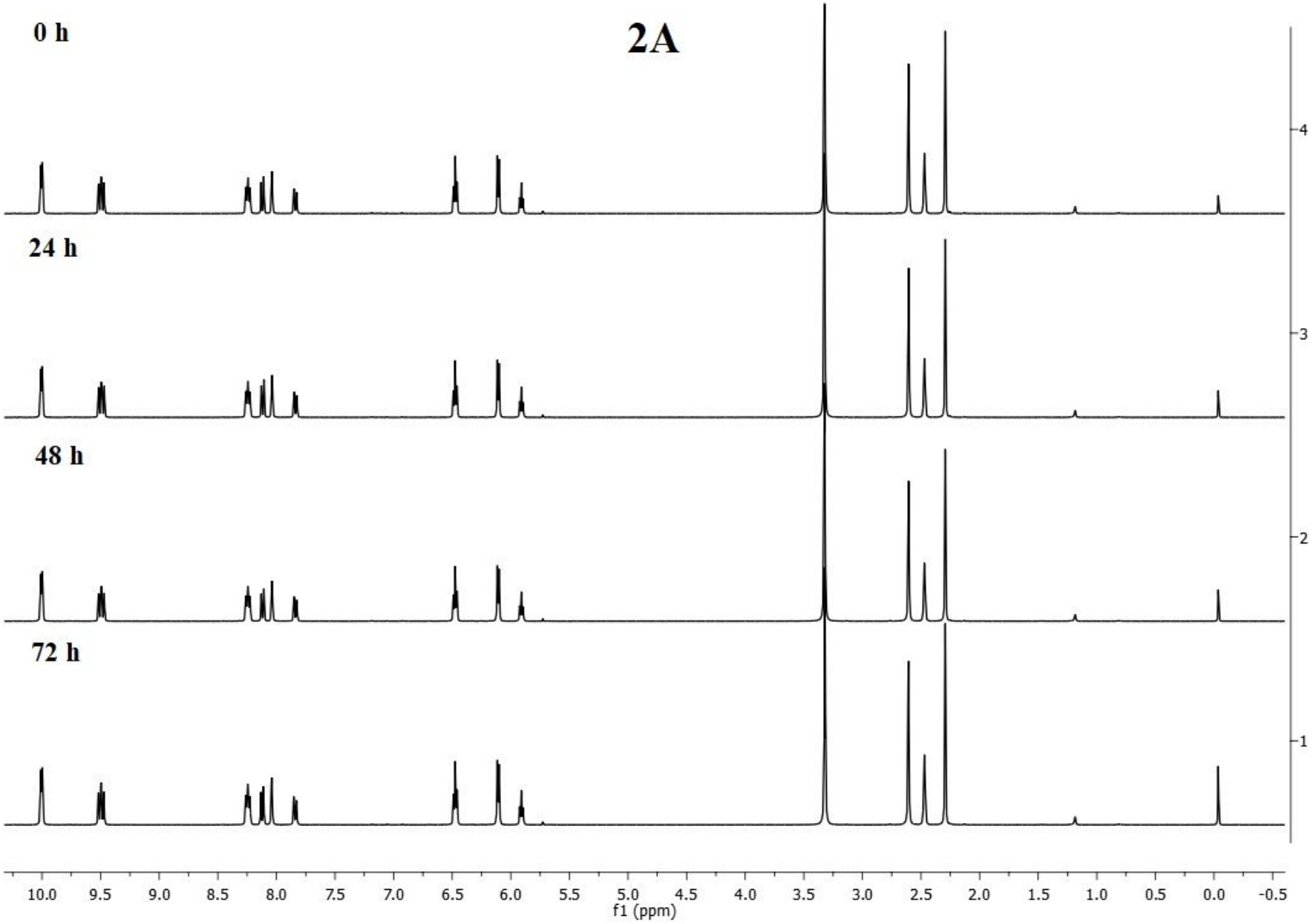

Figure S26. ^{1}H NMR study on the stability of **2A** in DMSO-d^{6} for 72 h.

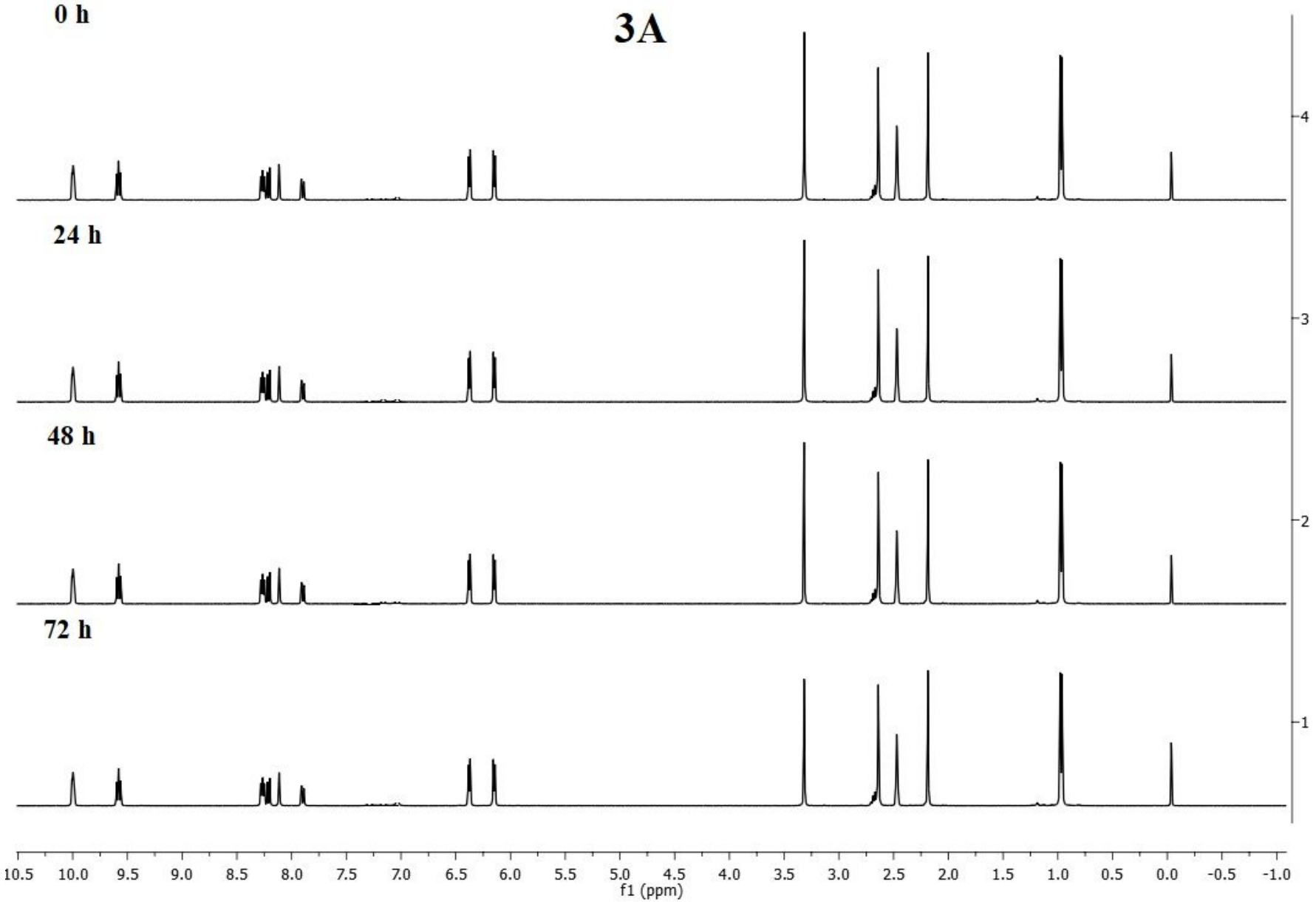

Figure S27. ^{1}H NMR study on the stability of **3A** in DMSO-d^{6} for 72 h.

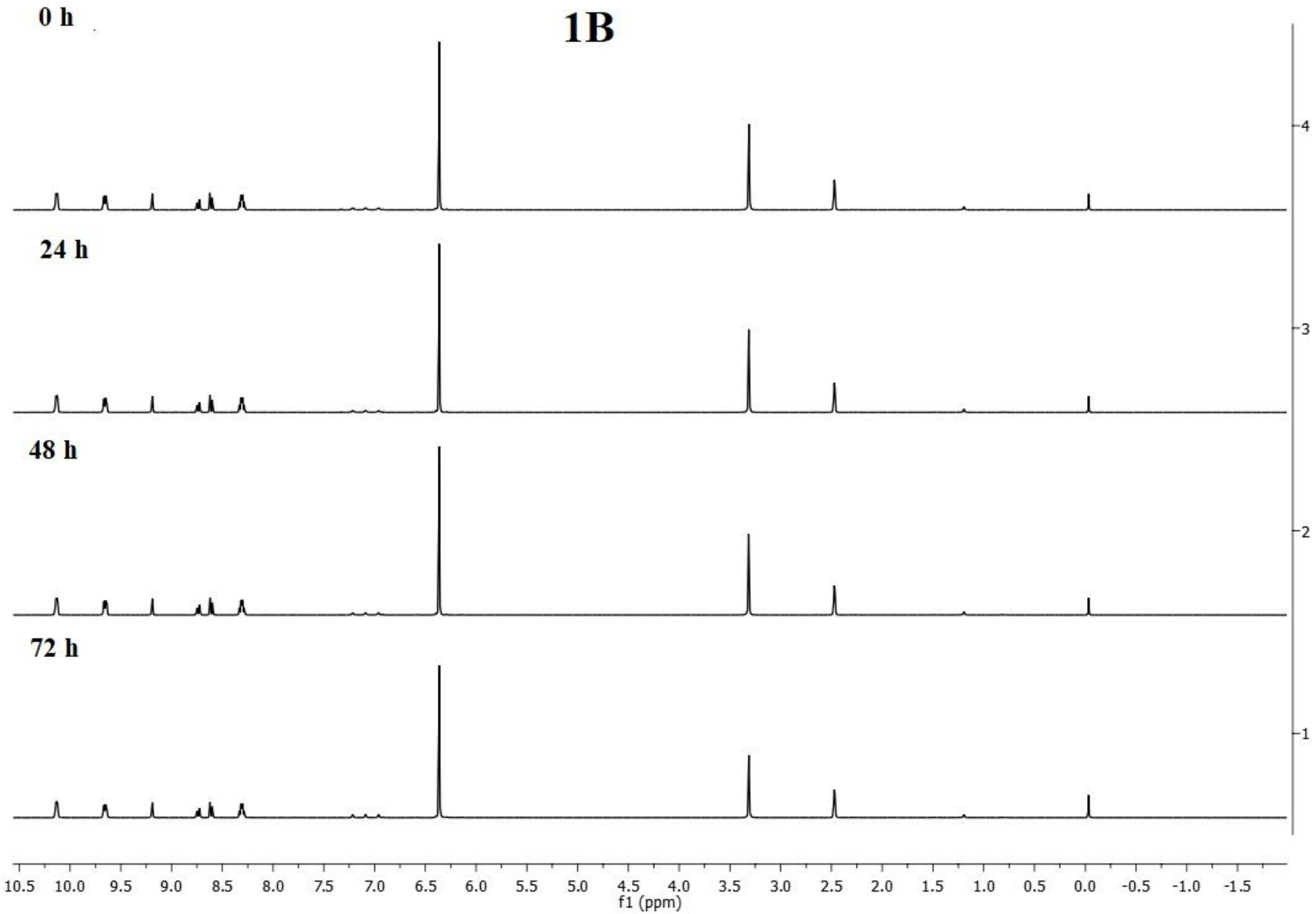

Figure S28. ^{1}H NMR study on the stability of **1B** in DMSO-d^{6} for 72 h.

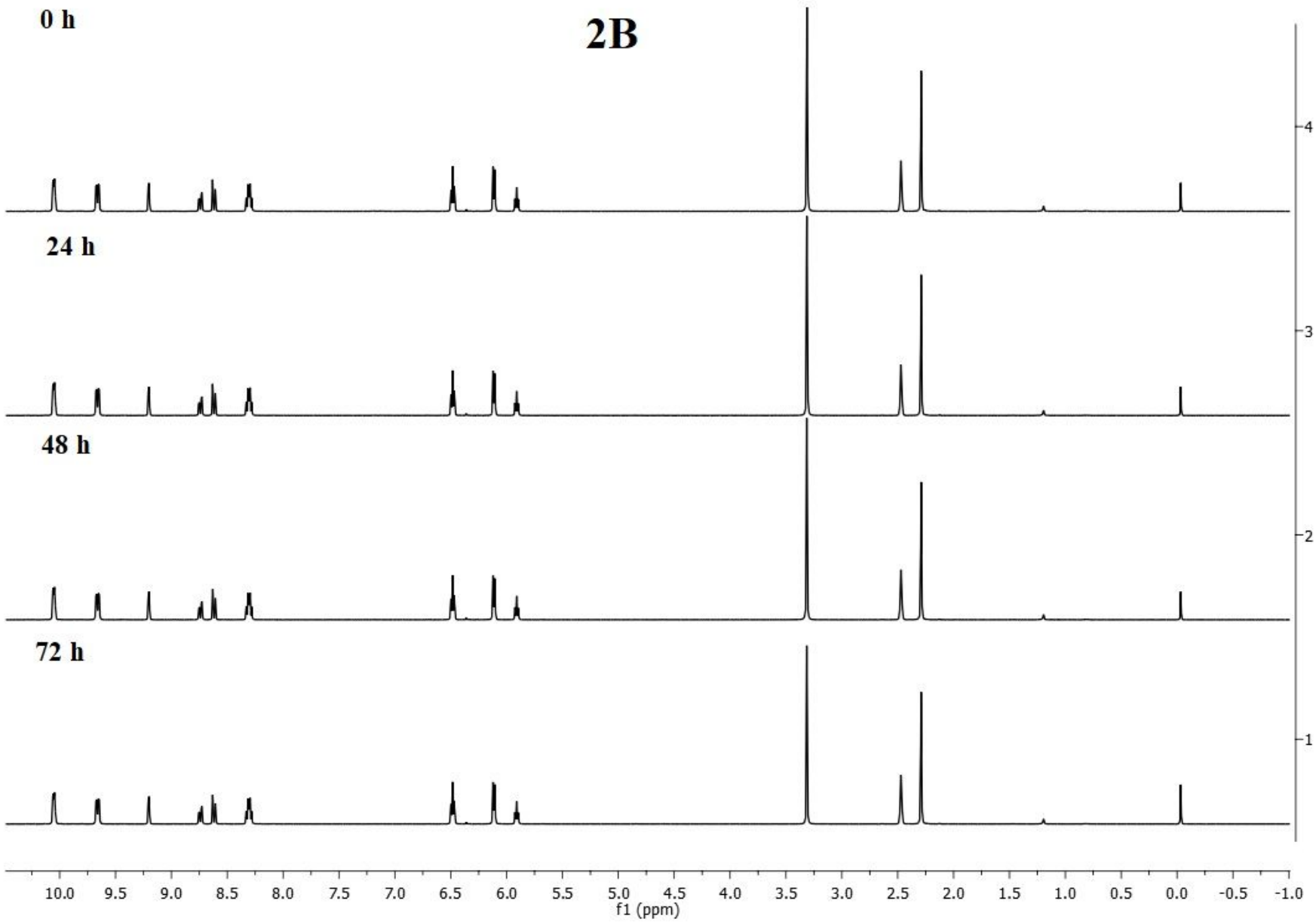

Figure S29. ^{1}H NMR study on the stability of **2B** in DMSO-d^{6} for 72 h.

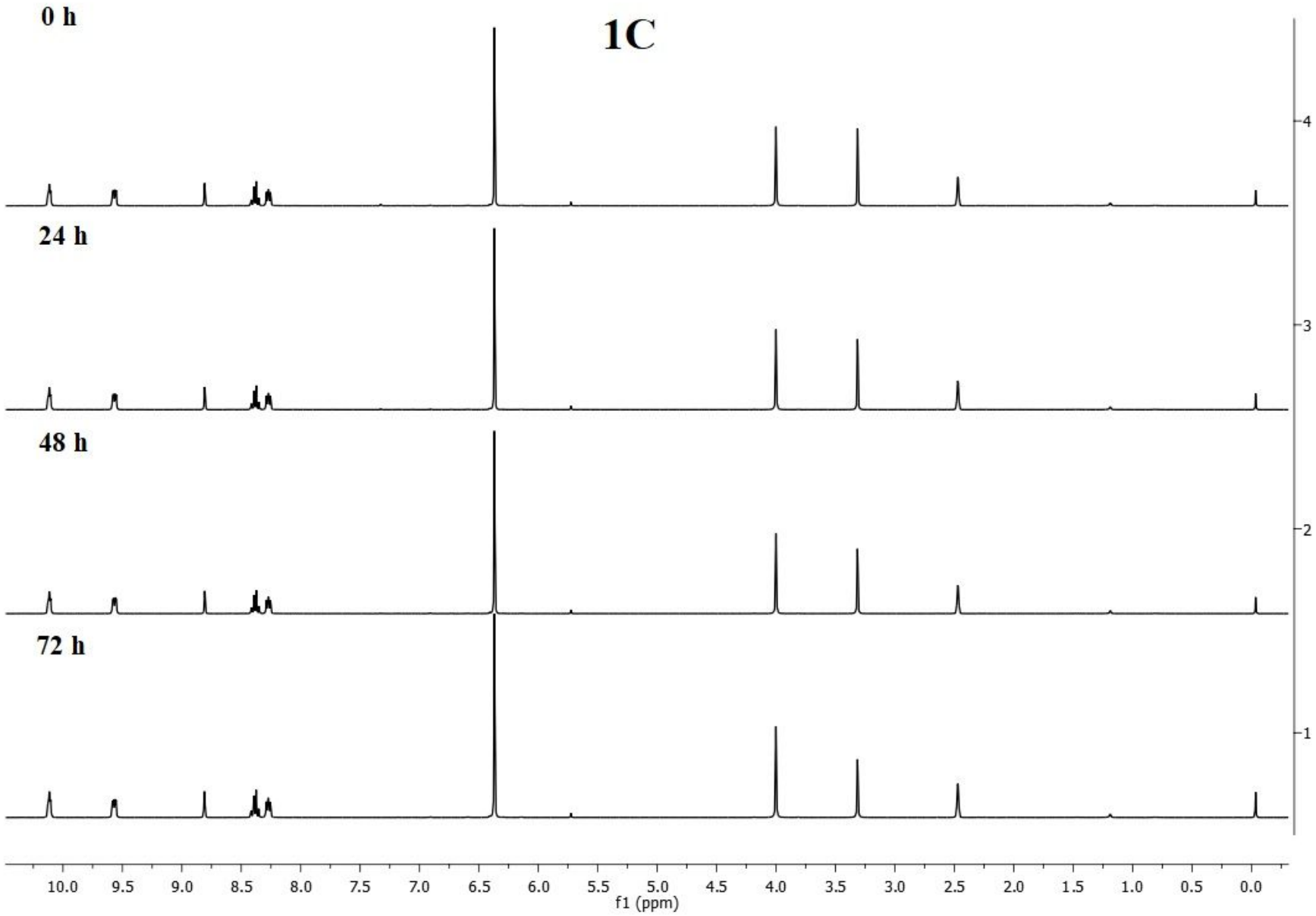

Figure S30. [1]H NMR study on the stability of **1C** in DMSO-d^6 for 72 h.

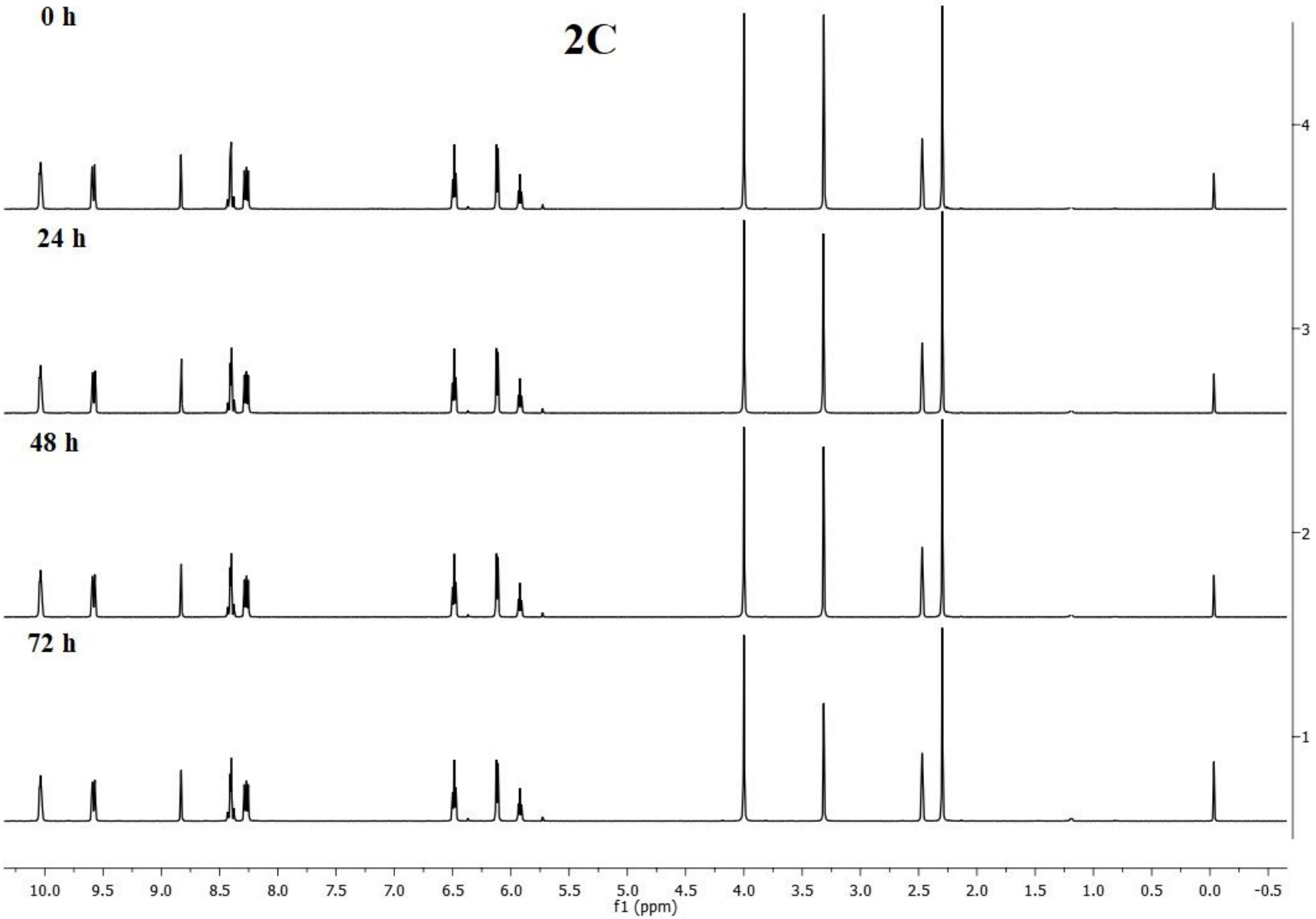

Figure S31. [1]H NMR study on the stability of **2C** in DMSO-*d*[6] for 72 h.

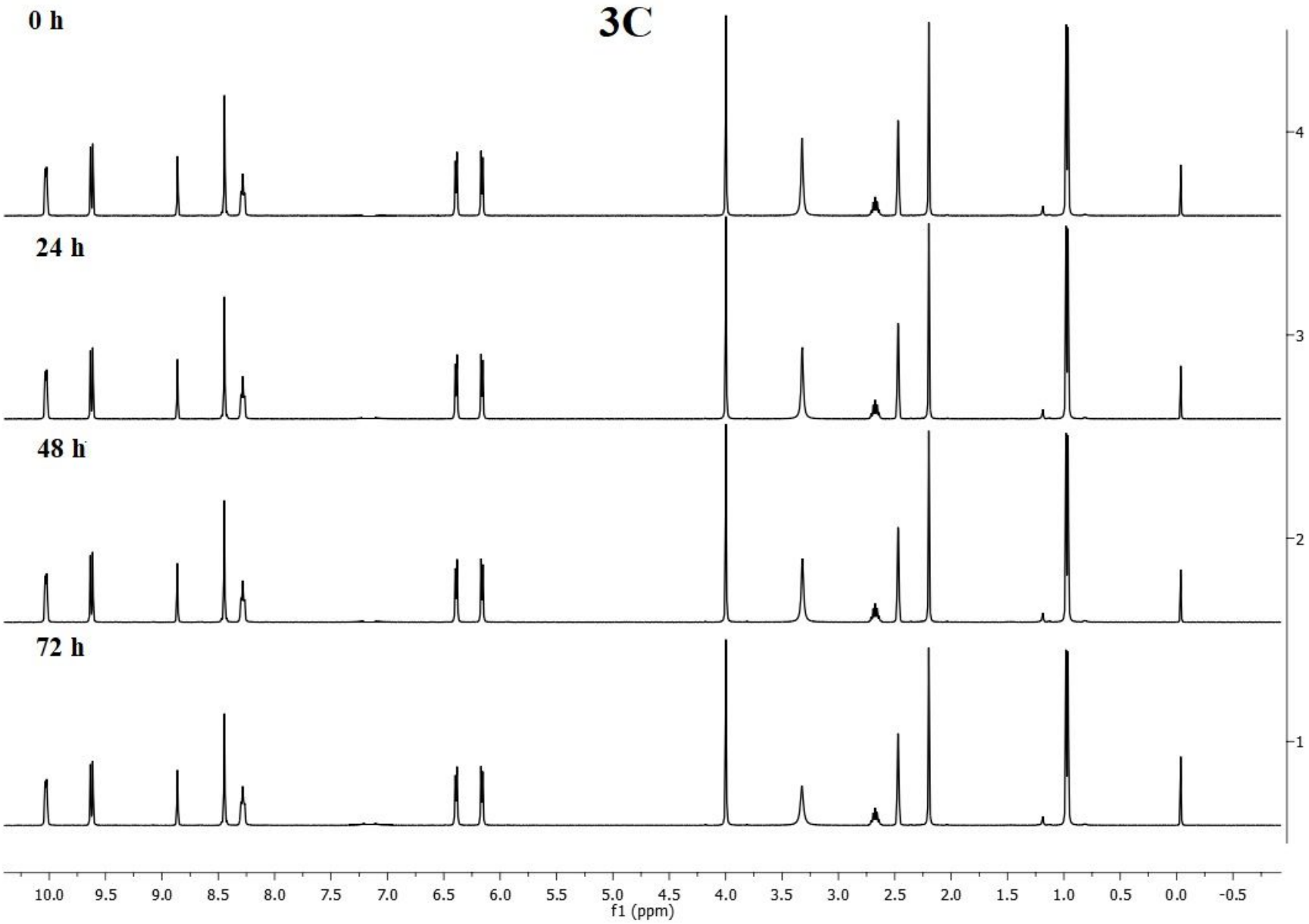

Figure S32. ^{1}H NMR study on the stability of **3C** in DMSO-d^{6} for 72 h.

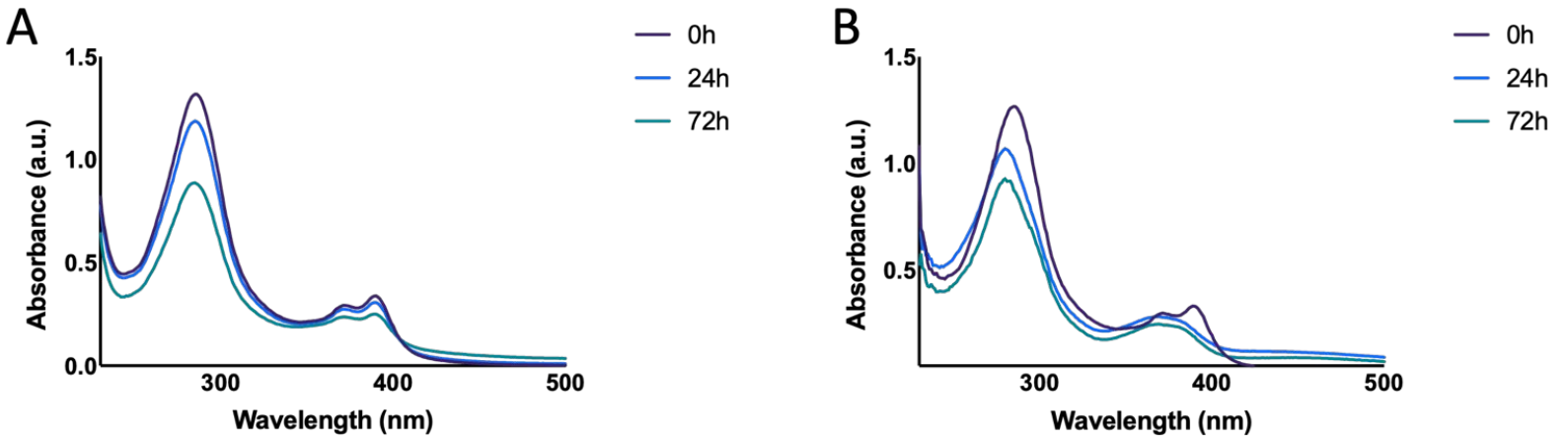

Figure S33. Stability of **1A** in 1% DMSO in PBS (A) and cell culture media (DMEM containing 10% FBS and 1% of Penicillin-Streptomycin (10,000 U/mL))/ H_2O in ratio 1:9 at 0, 24 and 72h.

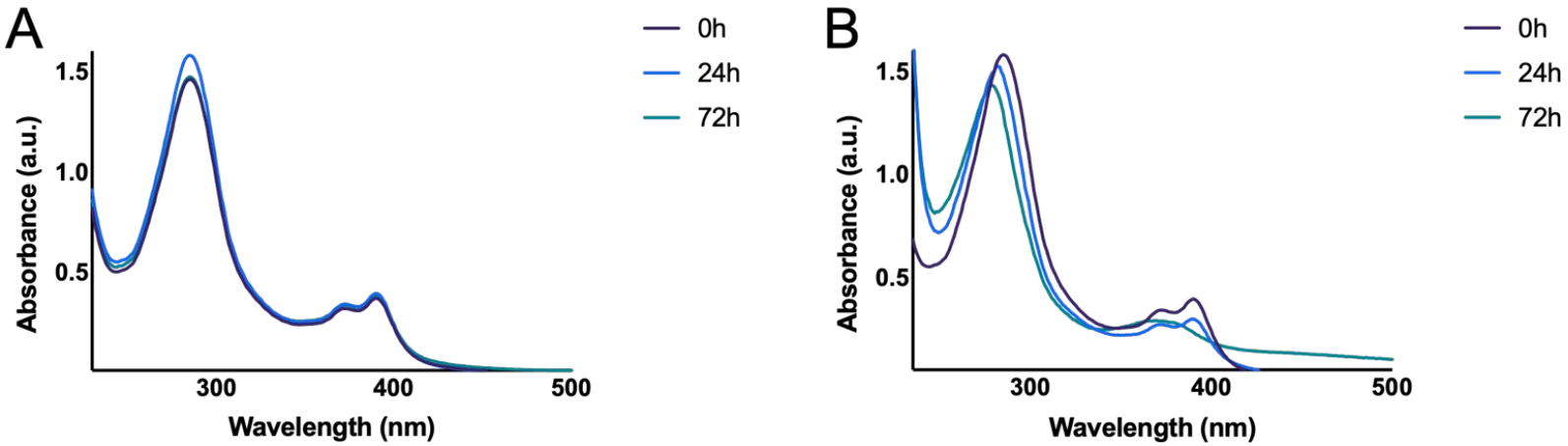

Figure S34. Stability of **2A** in 1% DMSO in PBS (A) and cell culture media (DMEM containing 10% FBS and 1% of Penicillin-Streptomycin (10,000 U/mL))/ H_2O in ratio 1:9 at 0, 24 and 72h.

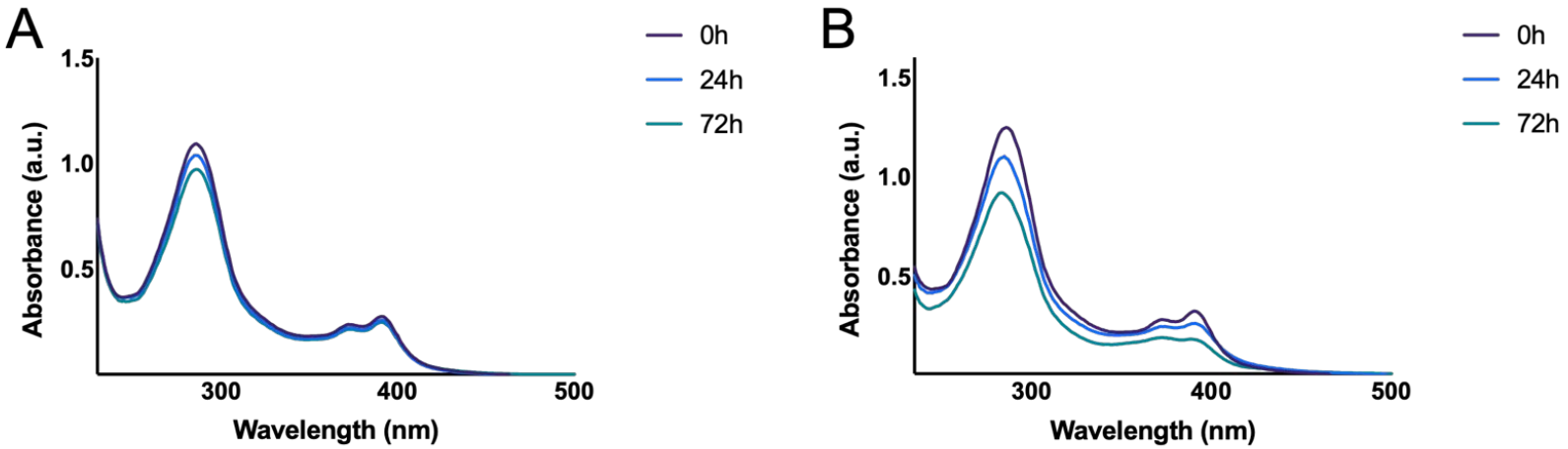

Figure S35. Stability of **3A** in 1% DMSO in PBS (A) and cell culture media (DMEM containing 10% FBS and 1% of Penicillin-Streptomycin (10,000 U/mL))/ H_2O in ratio 1:9 at 0, 24 and 72h.

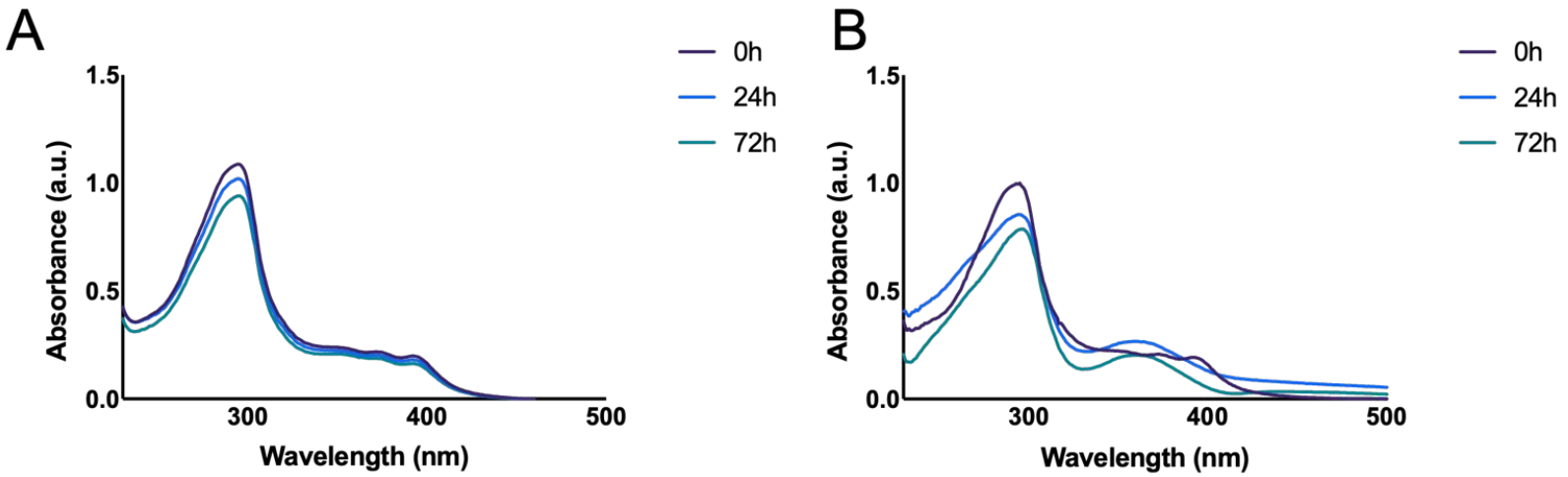

Figure S36. Stability of **1B** in 1% DMSO in PBS (A) and cell culture media (DMEM containing 10% FBS and 1% of Penicillin-Streptomycin (10,000 U/mL))/ H_2O in ratio 1:9 at 0, 24 and 72h.

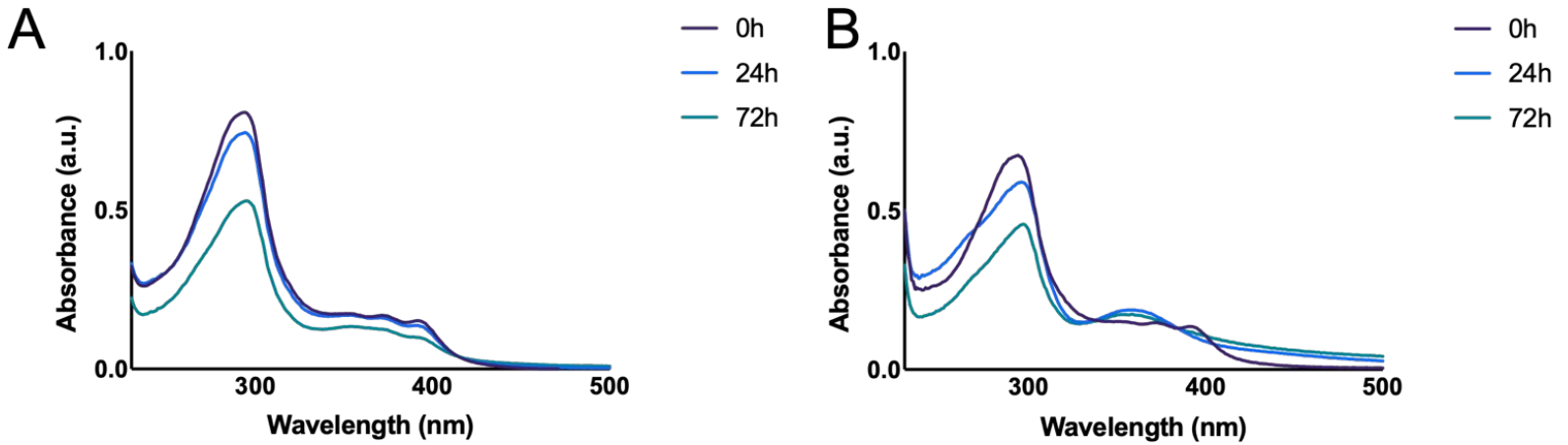

Figure S37. Stability of **2B** in 1% DMSO in PBS (A) and cell culture media (DMEM containing 10% FBS and 1% of Penicillin-Streptomycin (10,000 U/mL))/ H_2O in ratio 1:9 at 0, 24 and 72h.

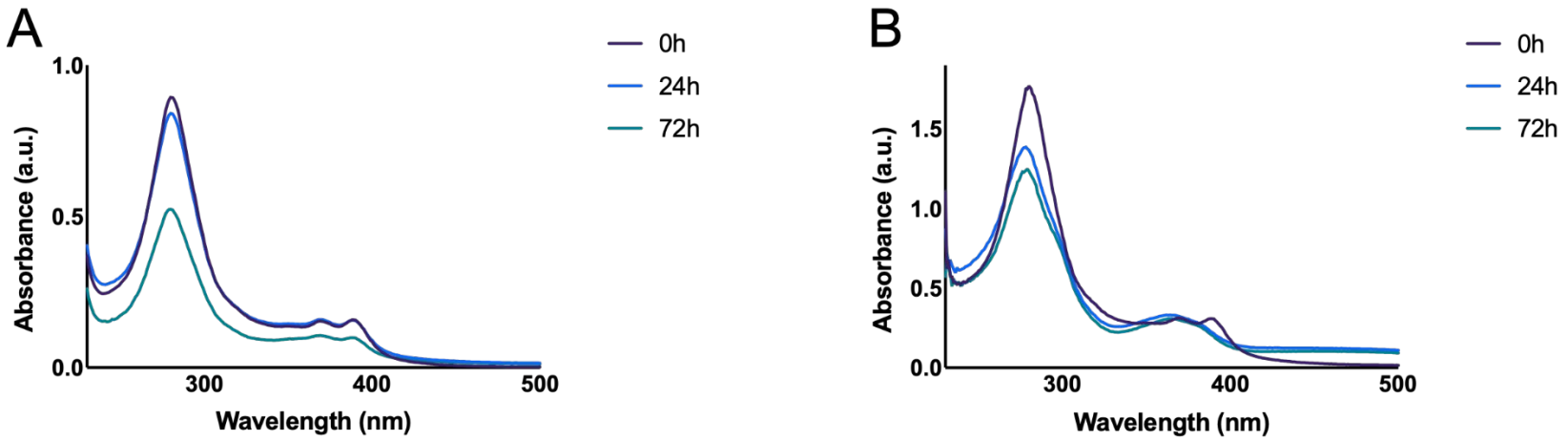

Figure S38. Stability of **1C** in 1% DMSO in PBS (A) and cell culture media (DMEM containing 10% FBS and 1% of Penicillin-Streptomycin (10,000 U/mL))/ H_2O in ratio 1:9 at 0, 24 and 72h.

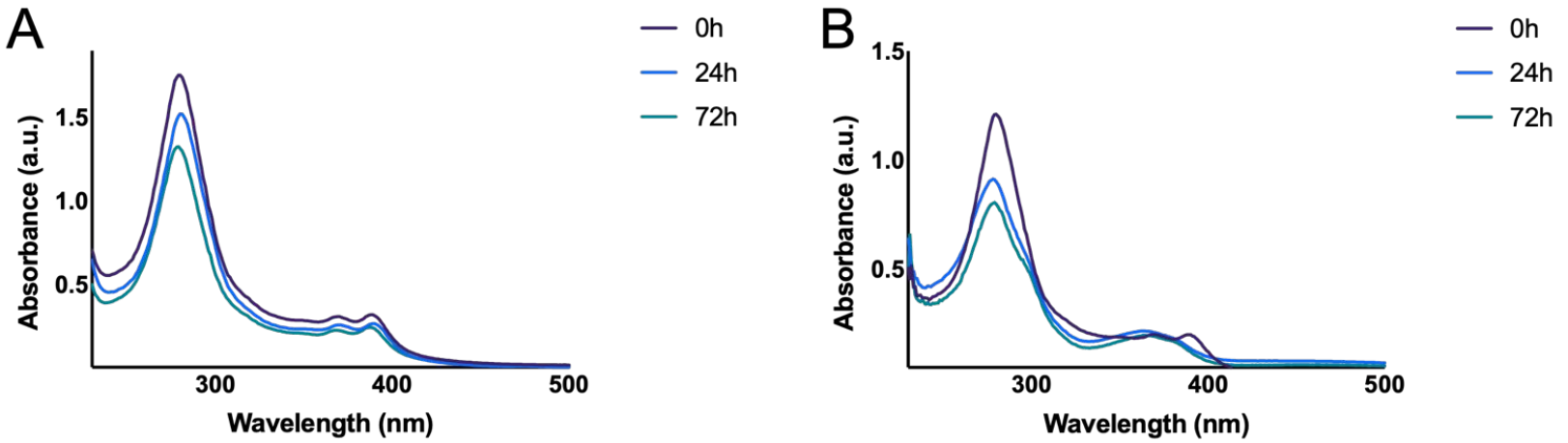

Figure S39. Stability of **2C** in 1% DMSO in PBS (A) and cell culture media (DMEM containing 10% FBS and 1% of Penicillin-Streptomycin (10,000 U/mL))/ H_2O in ratio 1:9 at 0, 24 and 72h.

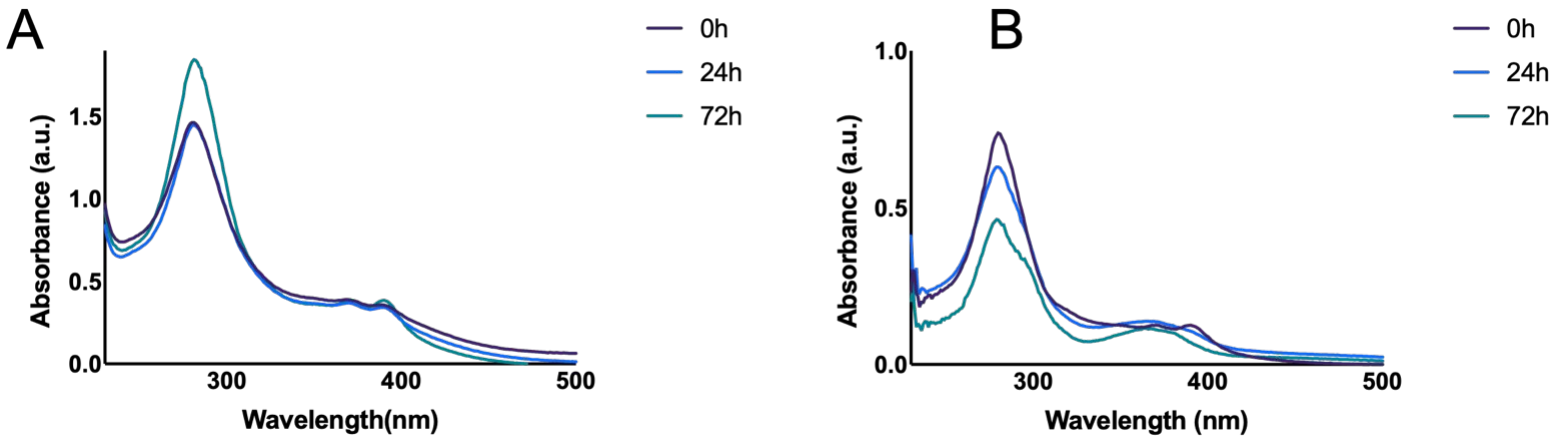

Figure S40. Stability of **3C** in 1% DMSO in PBS (A) and cell culture media (DMEM containing 10% FBS and 1% of Penicillin-Streptomycin (10,000 U/mL))/ H_2O in ratio 1:9 at 0, 24 and 72h.

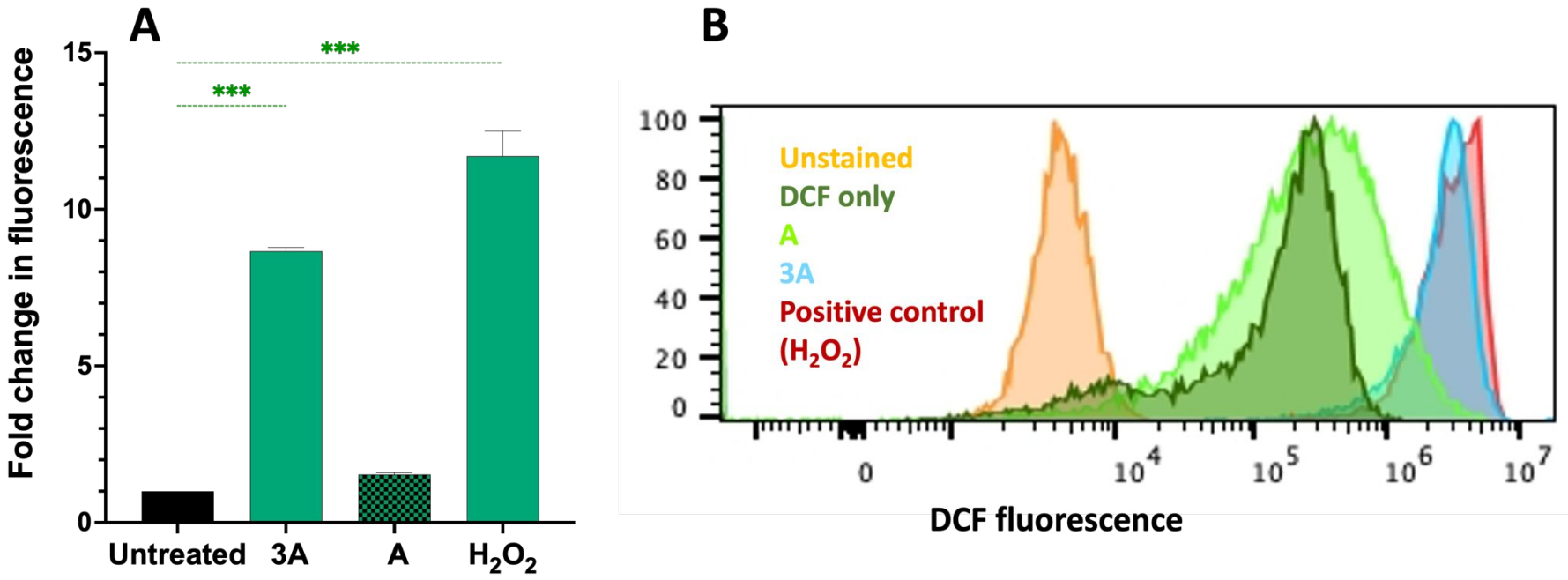

Figure S41. Flow cytometry analysis of intracellular ROS generation by **3A** and **A** by measuring the fluorescence intensity of DCF in FL-1 channel (excitation and emission wavelengths of 498 and 522 nm, respectively) in HCT116 cancer cells.

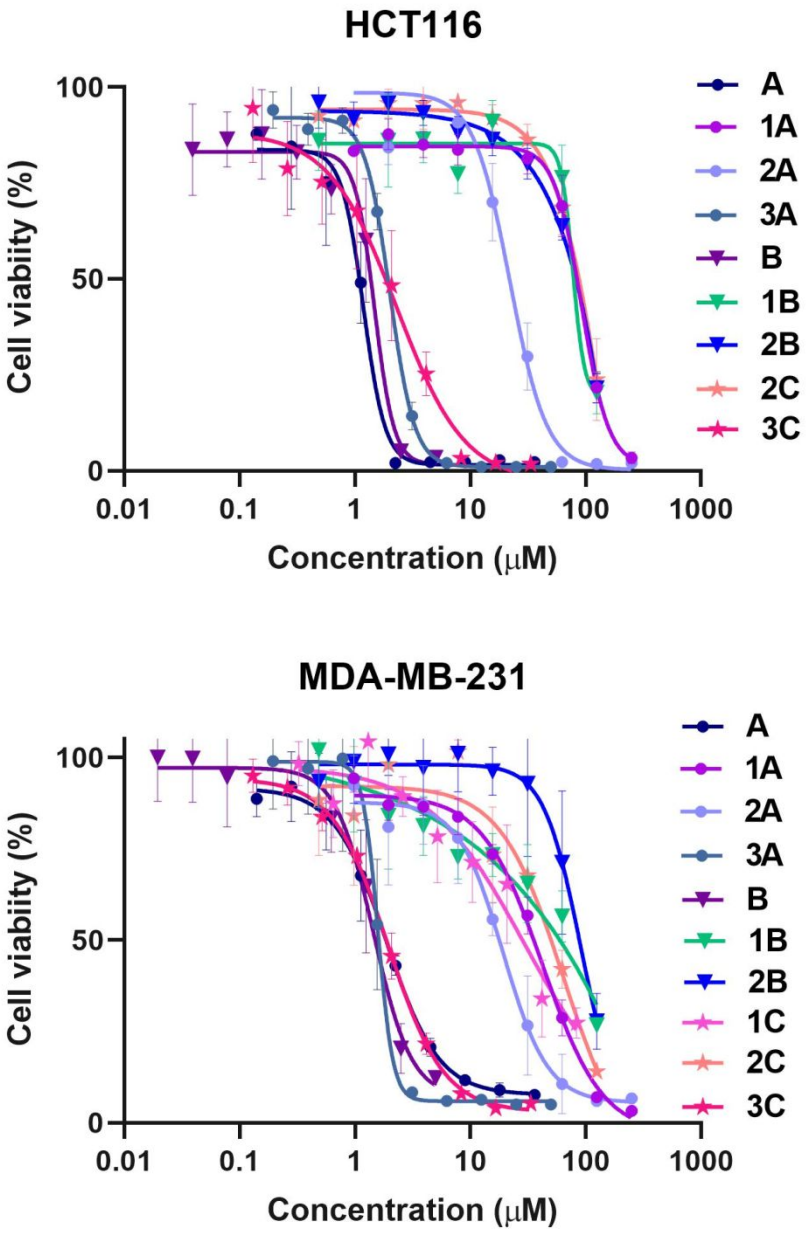

Figure S42. Concentration-effect curves for **1A-3A**, **1B**, **2B** and **1C-3C** in MDA-MB-231 and HCT116 cells lines upon 72 h exposure.

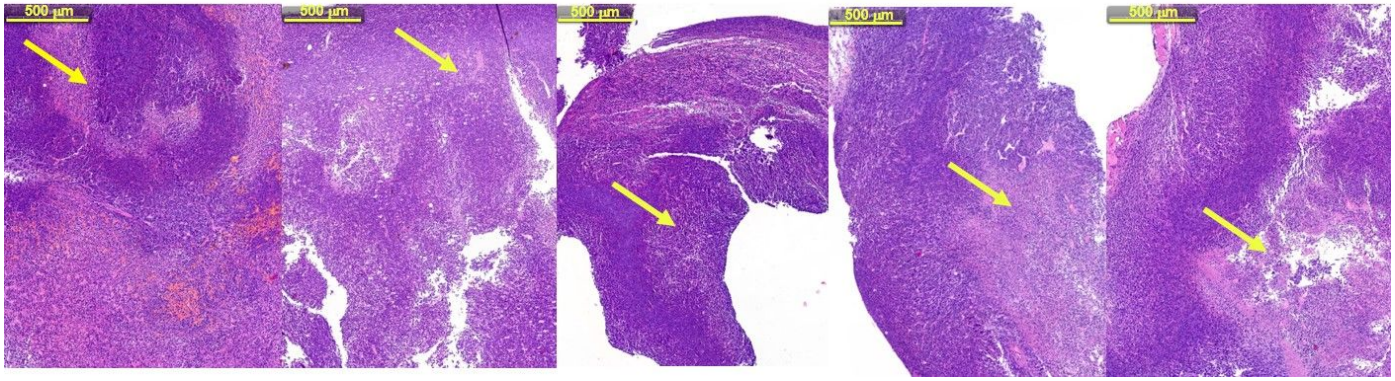

Figure S43. H&E-stained tumor sections in a Ru complex **3A**-treated group. Arrows indicate representative foci of necrosis. Histopathological analysis revealed solid sheets of high-grade carcinoma with low levels of necrosis. The scale bar represents 500 µm.

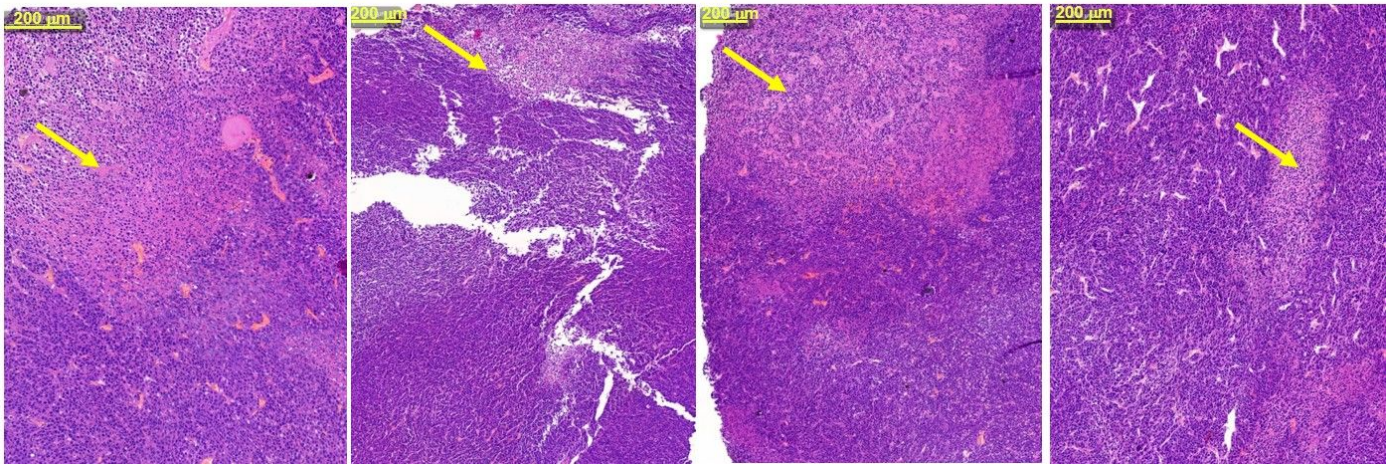

Figure S44. H&E-stained tumor sections in a vehicle-treated group. Arrows indicate representative foci of necrosis. Histopathological analysis revealed solid sheets of high-grade carcinoma with high levels of necrosis, characteristic for late stages of advanced solid tumors and highly proliferative tumors. The scale bar represents 200 µm.

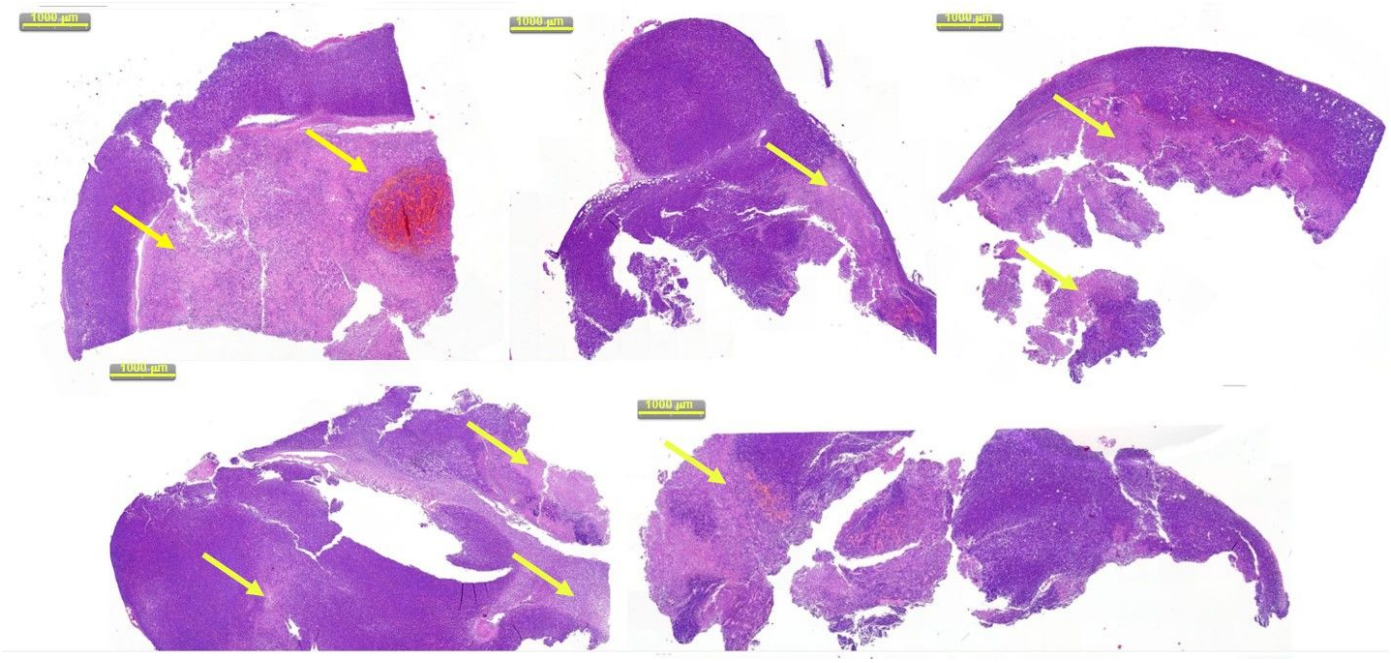

Figure S45. H&E-stained tumor sections in a ligand **A**-treated group. Arrows indicate representative foci of necrosis. Histopathological analysis revealed solid sheets of high-grade carcinoma with high levels of necrosis, characteristic for late stages of advanced solid tumors and highly proliferative tumors. The scale bar represents 1000 μm.

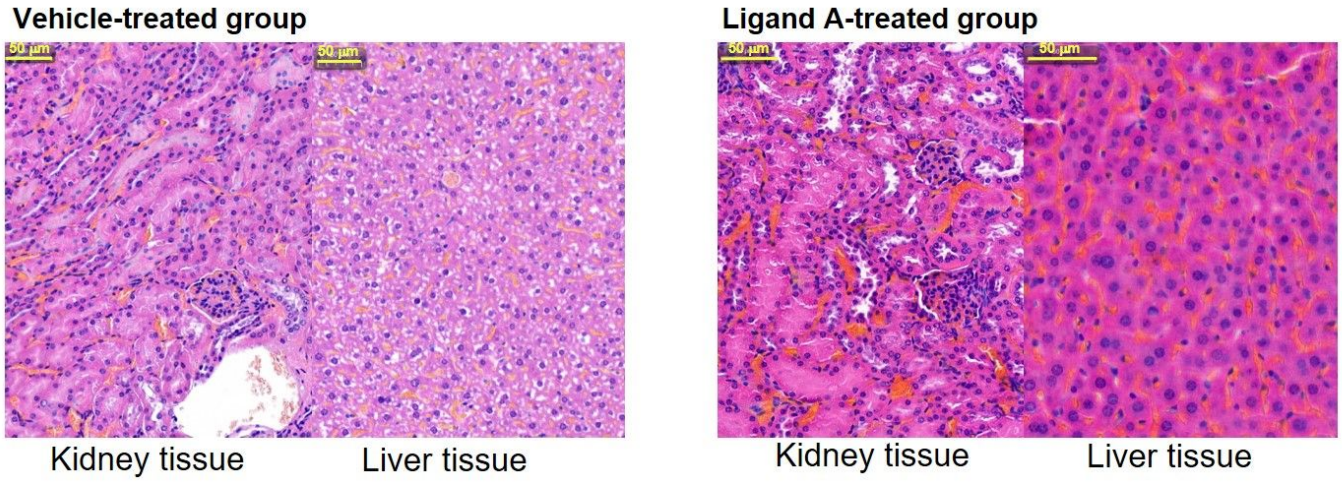

Figure S46. H&E-stained kidney and liver sections in a vehicle- and ligand **A**-treated groups. Histopathological analysis of kidney tissues revealed normal kidney structure without significant microscopic structural changes. Histopathological analysis of liver tissues in both groups revealed preserved liver tissue architecture with several areas of haemorrhages, nuclei polymorphism, sinusoidal dilatation and cytoplasm vacuolization. The scale bar represents 50 μm.